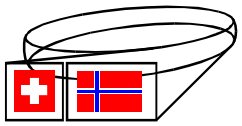

The Swiss - Norwegian Beam Lines
at ESRF

ACTIVITY REPORT

17/18

CONTENTS

SCIENTIFIC HIGHLIGHTS

ZINC FASTENS TWO AMYLOID-β PEPTIDE FRAGMENTS FORMING STABLE DIMER

Binding of metal ions to amyloid-β is an initial step of the peptide transition to pathogenic forms toxic for neurons. To understand the molecular mechanisms of zinc-mediated amyloid-β aggregation, amyloid-β peptide carrying a pathogenic Taiwanese mutation was studied. Spectroscopy showed that zinc ions induce formation of a stable homodimer with a novel binuclear zinc interaction fold.

Zinc ions are crucially involved in pathogenesis of Alzheimer's Disease (AD). This neurodegenerative disorder is characterised by extracellular accumulation of amyloid-β peptide (Aβ) in proteinaceous inclusions that have characteristic supramolecular structure and are abnormally enriched by Zn, Cu and Fe ions. Aβ interacts with metal ions through its metal-binding domain, which is located in its N-terminal region (residues 1-16). Substitutions and modifications of amino acid residues in this domain critically affect the properties of A-β, facilitating dimerisation, oligomerisation and the formation of insoluble aggregates. These processes are considered essential for the initiation of Alzheimer's disease.

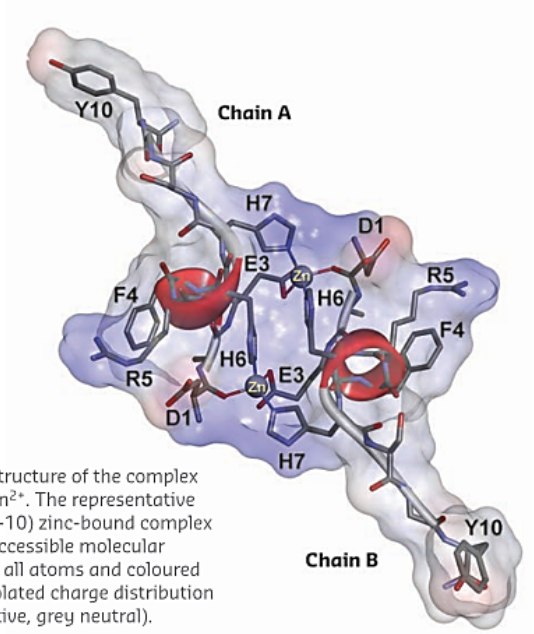

Fig. 19: NMR solution structure of the complex of D7H-Aβ(1-10) with Zn^{2+}. The representative conformer of D7H-Aβ(1-10) zinc-bound complex is shown. The solvent-accessible molecular surface is calculated for all atoms and coloured according to the interpolated charge distribution (red negative, blue positive, grey neutral).

Aβ carrying a Taiwanese mutation (D7H) stands out among all isoforms of Aβ because of the enhanced susceptibility of the peptide to the effect of Zn^{2+} or Cu^{2+} ions promoting oligomerisation **[1]**. Based on the molecular mechanism of formation of zinc-bonded dimers of different Aβ isoforms **[2]**, it was hypothesised that zinc-dependent aggregation of the metal-binding domain of Aβ with Taiwanese mutation is determined by the properties of the fragment containing residues 1-10 (D7H-Aβ(1-10)), where the relevant amino acid substitution is located.

In this study, using NMR spectroscopy, mass spectrometry, EXAFS spectroscopy on **BM31** and isothermal titration calorimetry (ITC), the behaviour of this peptide fragment in the presence of zinc ions was examined. The formation of a homodimer with a unique protein fold interlocked by two zinc ions (**Figure 19**) was observed by NMR. Most of the known examples of metal-directed peptide self-assembly are

based on the formation of one or several mononuclear coordination sites. Examples of the formation of a binuclear coordination site with the participation of two zinc ions are still unknown, except when cysteine thiol groups are involved in the binding of zinc atoms.

It has been shown here for the first time that a site, with a novel topology for the coordination sphere of zinc ions, is formed upon the interaction of zinc with a relatively short fragment of A-β peptide carrying Taiwanese mutation D7H. The NMR structure determined was validated using extended X-ray absorption fine structure (EXAFS) spectroscopy, which provides information on the geometry of the metal ion chelating environment. EXAFS data give access to the nature, number, and distance of the coordinating atoms. The experimental EXAFS spectrum of the complex of D7H-Aβ(1-10) with zinc fits well to the spectrum, calculated on the basis of the coordinates of atoms determined by NMR (**Figure 20**). The scattering pathways for the atoms of the first coordination shell (D1 O, E3 Oε1, H6 Nε2 and H7 Nε2) reproduce the most intense peak at ~2 Å of the Fourier-transformed EXAFS spectrum (**Figure 20c**), while atoms of the histidine imidazole ring make a major contribution to the peaks at ~3 Å and ~4 Å.

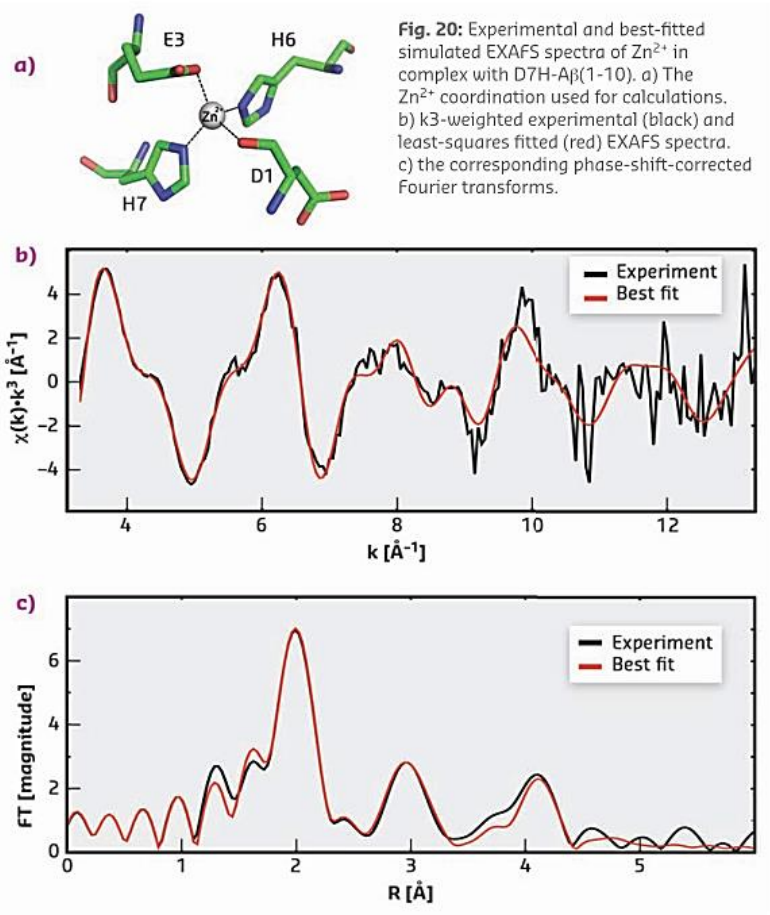

Fig. 20: Experimental and best-fitted simulated EXAFS spectra of Zn^{2+} in complex with D7H-Aβ(1-10). a) The Zn^{2+} coordination used for calculations. b) k3-weighted experimental (black) and least-squares fitted (red) EXAFS spectra. c) the corresponding phase-shift-corrected Fourier transforms.

PRINCIPAL PUBLICATION AND AUTHORS

A Binuclear Zinc Interaction Fold Discovered in the Homodimer of Alzheimer's Amyloid-β Fragment with Taiwanese Mutation D7H, V.I. Polshakov (a,b), A.B. Mantsyzov (b), S.A. Kozin (a), A.A. Adzhubei (a), S.S. Zhokhov (b), W. Van Beek (c), A.A. Kulikova (a), M.I. Indeykina (d), V.A. Mitkevich (a) and A.A. Makarov (a), *Angew. Chem. Int. Ed.* **56**, 11734-11739 (2017); doi: 10.1002/anie.201704615.
(a) Engelhardt Institute of Molecular Biology, Russian Academy of Sciences, Moscow (Russia)
(b) Faculty of Fundamental Medicine, M.V. Lomonosov Moscow State University, Moscow (Russia)
(c) SNBL, ESRF
(d) Emanuel Institute for Biochemical Physics, Russian Academy of Sciences, Moscow (Russia)

REFERENCES

[1] W.-T. Chen *et al., PLoS One* **7**, e35807 (2012).
[2] A.N. Istrate *et al., Sci. Rep.* **6**, 21734 (2016).

ELASTIC PROPERTIES REVEALED BY THERMAL DIFFUSE SCATTERING

The full elasticity tensor can be obtained in a single crystal diffraction experiment through measurement of thermal diffuse scattering. Both the elastic properties and the crystal structure are determined by this new approach.

Elastic moduli give important insights into the mechanical behaviour of crystalline materials. Accurate measurements of the elasticity tensor – which contains the full set of elastic moduli – are of principal interest in materials science, geophysics and condensed matter physics. Applications include superconductors, low dimensional spin systems and an improved understanding of seismological wave propagation, which, in turn, allows for decisive conclusions on composition, temperature and pressure of the Earth's interior.

The two most commonly used experimental techniques to determine the elastic tensor are ultrasound measurements and Brillouin scattering. While the former has strong limitations on small crystals and experiments under extreme conditions, the latter is difficult for opaque materials. Alternatively, information on the elasticity tensor can be obtained from inelastic scattering experiments. Now, it has been shown that the full elasticity tensor can be determined by high-precision measurements of thermal diffuse scattering from a single crystal, thus opening new perspectives in a range of scientific fields.

Thermal diffuse scattering arises from the vibrations of atoms around their equilibrium positions. In a scattering experiment these vibrations result in intensities in between Bragg reflections and are the fingerprints of the lattice dynamics. In the vicinity of Bragg reflections, the scattering intensities are dominated by acoustic phonons that correspond to elastic waves. These waves propagate with the speed of sound that can take different values depending on the composition, the crystal symmetry, direction and external influences such as temperature and pressure. The full information is given by the elasticity tensor, which can be extracted by a careful analysis of the scattering intensities.

High-quality single crystals of magnesium oxide and calcite are investigated as benchmark systems. The experimental setup is illustrated in Figure 91. Scattering intensities were collected at beamlines **ID29** and **BM01A**. The sample was rotated with angular steps of 0.1° with

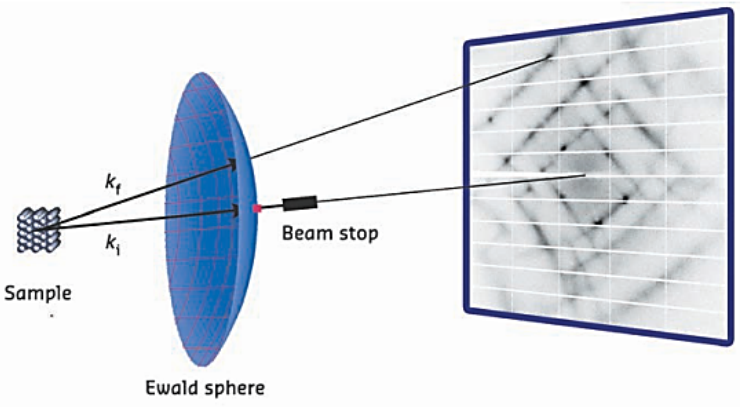

Fig. 91: Diffraction geometry for a diffuse scattering experiment in transmission **[1]**. The incoming monochromatic X-rays with wave vector k_i are scattered by the sample and diffracted onto the Ewald sphere. The area detector records the planar projection of the Ewald sphere.

Calcite			Magnesium oxide			
	TDS	US		TDS	US	
	T = 170 K			I(T = 120 K) – I(T = 90 K)	T = 90 K	T = 120 K
C_{11}	156	155.1	C_{11}	300	306.1	305.4
C_{13}	57.0	57.69	C_{44}	151	157.2	156.9
C_{15}	21.2	21.51	C_{12}	89	94.07	94.26
C_{33}	87.6	87.12				
C_{44}	35.7	34.42				
C_{66}	48.0	47.80				

Table 1: Elastic moduli of calcite and magnesium oxide determined from thermal diffuse scattering (TDS) and ultrasound measurements (US). Values are given in GPa.

exposure times adapted to the weak diffuse scattering. Measurements were taken at various temperatures. Details of the experimental setup and the underlying theory can be found elsewhere **[1, 2]**.

The data treatment required a novel analysis technique and the development of a specialised software package, which comprises the precise reconstruction of reciprocal space and careful selection of regions in reciprocal space to be treated. The software simultaneously fits approximately 10^7 individual intensity points by taking into account the exact scattering geometry and symmetry of the crystal.

Determination of the elastic moduli from thermal diffuse scattering measured at a single temperature is demonstrated for a small calcite single crystal. Experimental scattering intensities and calculated thermal diffuse scattering intensities from the fitted elastic moduli are compared in **Figure 92**. Remarkably, the results agree within about 1% with values determined by ultrasound measurements (see **Table 1**).

Absolute values of the elastic moduli can be obtained if measurements are taken at slightly different temperatures. This strategy further allows separation of the inelastic contribution from elastic scattering that may arise from disorder or imperfect surfaces. This is shown for magnesium oxide (see **Table 1**), for which accurate values in absolute units were obtained by fitting scattering intensities at two temperatures.

The new method is model-free and can be applied to very small and opaque crystals of arbitrary shape and symmetry. This implies a broad applicability in material science, geophysics and in the study of sound wave anomalies due to fundamental interactions in condensed matter physics. It is possible to measure the elastic properties together with the crystal structure in the same experiment. This is a great benefit for measurements at extreme conditions, such as high pressures, where it is often difficult to reproduce the exact experimental conditions.

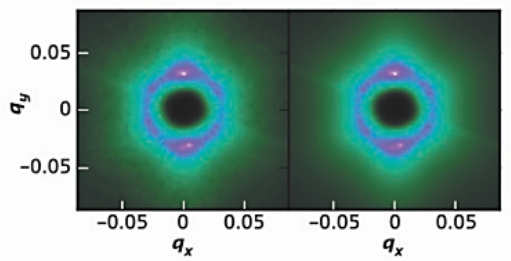

Fig. 92: Measured (left panel) and calculated (right panel) thermal diffuse scattering from calcite (T = 170 K) for momentum transfers $q \in [0.03, 0.15]$. The images show a cross-section of the reciprocal space in Cartesian coordinates, in the neighbourhood of the Bragg peak $[\bar{1}, 0, \bar{16}]$ with $q_z = 0$. The scattering intensity is shown on a linear colour scale from black (zero) to white (maximum intensity).

PRINCIPAL PUBLICATION AND AUTHORS

Full elasticity tensor from thermal diffuse scattering, B. Wehinger (a,b), A. Mirone (c), M. Krisch (c) and A. Bosak (c), *Physical Review Letters* **118**, 035502 (2017); doi: 10.1103/PhysRevLett.118.035502.

(a) Department of Quantum Matter Physics, University of Geneva (Switzerland)
(b) Laboratory for Neutron Scattering and Imaging, Paul Scherrer Institute, Villigen (Switzerland)
(c) ESRF

REFERENCES

[1] B. Wehinger, PhD thesis, Université de Grenoble (2013), http://tel.archives-ouvertes.fr/tel-00961602.
[2] A. Bosak *et al.*, *Journal of Physics. D, Applied Physics* **48**(50), 50400 (2015).

Understanding the Structure of Layered Cuprate Thin Films

H. H. Sønsteby, J. E. Bratvold, K. Weibye, H. Fjellvåg, O. Nilsen
University of Oslo, Department of Chemistry, Norway

Perovskite-related layered cuprates are considered the basis of conventional high-Tc superconductors. These strongly correlated materials have been studied for decades, but much still remains to be understood about the unusual interplay between their structure and properties. Epitaxial thin films of layered complex cuprates where the weakly coupled copper planes are oriented in the substrate surface plane are especially interesting. This is due to the simplified deconvolution of directionally dependent properties.
One of the strategies is to study the mother system of this material type: Perovskite $MCuO_{3-x}$. $LaCuO_{3-x}$ is considered one of the most promising systems in this respect. It exhibits a large versatility in oxygen off-stoichiometry and could help shed light on the role played by the mixture of Cu^{3+} and Cu^{2+} that is found in most high-T_c superconductors. Copper valence in $LaCuO_{3-x}$ can be varied from only Cu^{2+} in insulating orthorhombic $LaCuO_{2.5}$ (*i.e.* $La_2Cu_2O_5$) all the way to only Cu^{3+} in metallic tetragonal $LaCuO_3$. A metallic monoclinic phase exists for the interval $0.1 < x < 0.5$. (Figure 1). Studying the structure and properties of the intermediary valence compounds could help explain some of the strong correlation in these material types.

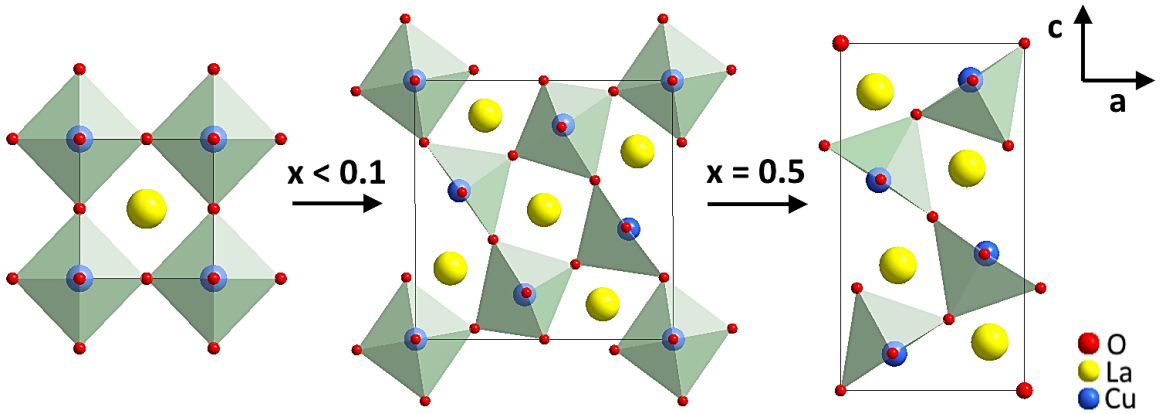

Figure 1: The three different structures of $LaCuO_{3-x}$ found at different understoichometries of oxygen.

Unfortunately, layered cuprates are not the most straightforward type of material to deposit as thin films, especially by chemical methods. Copper oxides are notorious for catalytic decomposition of metal-organic precursors, which are used in techniques like CVD. This results in loss of compositional control during the growth phase.
In this study, we utilized the self-limiting nature of the atomic layer deposition (ALD) technique to overcome these challenges. We showed that careful control of the copper precursor flux, precursor sublimation temperature and deposition temperature enables unmatched control of stoichiometry and uniformity in these thin films. Epitaxial thin films of $LaCuO_{3-x}$ (001) were deposited on single crystal substrates of $LaAlO_3$ $(100)_{pc}$, using commercially available cation precursors $(La(thd)_3$ and

$Cu(acac)_2$). Ozone was used as oxygen source to get strongly a strongly oxidizing environment.

The thin films are amorphous as deposited by ALD, and a post-deposition annealing step is necessary to obtain crystalline films. The $LaAlO_3$ $(100)_{pc}$ substrates facilitate oriented crystallization, with the (001)-planes of $LaCuO_{3-x}$ oriented parallel to the film surface.

Different annealing parameters were used to enable control of the oxygen stoichiometry. Annealing in air at 650 °C for 15 minutes resulted in phase-pure, oriented, crystalline films. Annealing in oxygen at 900 °C for 10 hours increased the crystallinity, but from specular diffraction it was not possible distinguish if the two treatments resulted in different crystal structures.

Diffraction from the three variants of $LaCuO_{3-x}$ is very similar, and all specular reflections in from (00*l*)-planes are close to equal. Observing significant differences is only possible by moving far out in the reciprocal space. We noted that a (640) reflection close to the substrate $(310)_{pc}$ would exist for the monoclinic phase, with no reflections from the orthorhombic phase nearby.

Studying this requires a diffraction setup that covers a relatively large q-range, and an area detector with sufficient resolution to deconvolute the $LaCuO_{3-x}$ (640) and $LaAlO_3$ $(310)_{pc}$ reflections. The versatile setup at the Swiss Norwegian Beam Lines (BM01) offers the possibility to carry out these kinds of experiments. A flexible goniometer together with the Pilatus 2M detector gives the perfect conditions to study these small variations.

We identified the substrate (310) reflections, and carried out a high resolution reciprocal space mapping around this reflection for both air annealed and oxygen annealed samples (Figure 2). It is immediately clear that the (640)-reflection from the monoclinic structure only exists for the oxygen-annealed sample.

By using x-ray photoelectron spectroscopy, the oxygen content was crudely estimated to $x = 2.67$ for the oxygen annealed sample. Furthermore, 4-point probe resistivity measurements showed that the air-annealed samples are insulating, whereas oxygen annealed samples exhibit metallic conductivity.

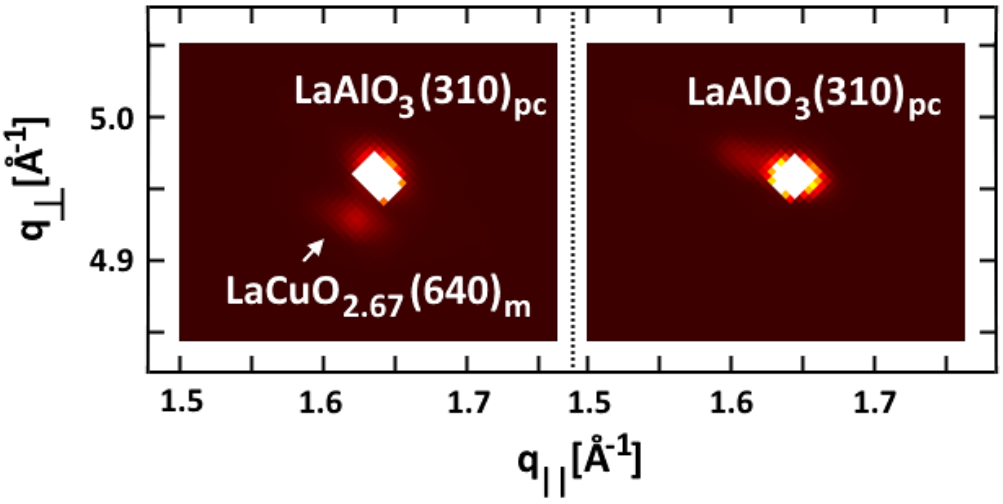

Figure 2: Reciprocal space maps around the substrate $LaAlO_3$ $(310)_{pc}$ for the oxygen-annealed (left) and air annealed (right) $LaCuO_{3-x}$ films. The substrate peak is pixelated due to overexposure.

All these observations support our conclusions: Control of the chemistry and structure of thin films of $LaCuO_{3-x}$ can be obtained by careful selection of deposition parameters and post annealing conditions. The versatility of BM01 proved an essential tool in understanding these structures. We believe that the ability to probe the properties of these different structure types may prove important to understand the underlying mechanisms behind the properties of layered cuprate systems.

Principal publication and authors

Phase Control in Thin Films of Layered Cuprates, H. H. Sønsteby[(a)], J. E. Bratvold[(a)], K. Weibye[(a)], H. Fjellvåg[(a)], O. Nilsen[(a)], *Chem. Mater.*, **8,** 1095 (2018), doi: 10.1021/acs.chemmater.7b05005
(a) University of Oslo, Department of Chemistry, Norway

References

[1] Sønsteby *et al.*, *Adv. Mater. Interfac.* **4**, 1600903 (2017)
[2] Sønsteby *et al*., *Chem. Comm.* **54**, 8253 (2018)

Structure and interstitial iodide migration in hybrid perovskite methylammonium lead iodide

J. L. Minns[a], P. Zajdel[b], D. Chernyshov[c], W. van Beek[c] & M. A. Green[a]

[a]*School of Physical Sciences, Ingram Building, University of Kent, Canterbury, Kent CT2 7NH, UK.*
[b]*Institute of Physics, University of Silesia, ul. Uniwersyteck, 4, 40007 Katowice, Poland.*
[c]*Swiss-Norwegian Beam Lines, European Synchrotron Radiation Facility, Polygone Scientifique Louis Ne´el, 6, Rue Jules Horowitz,38000 Grenoble, France*

Perovskite structures, with the general formula, ABO_3, form one of the most important and commercially exploited family of solids. Hybrid perovskites that contain both organic and inorganic components are a subset, where the A site is composed of an organic cation, such as methylammonium (MA), within a post transition metal halide framework, such as lead iodide. They have emerged since 2009 [1] as simple, low cost solar cell materials, with power conversion efficiencies that are becoming competitive with silicon [2-5]. Methylammonium lead iodide (MAPbI) undergoes a number of structural phase transitions as a function of temperature, including an orthorhombic—tetragonal—cubic evolution that is common in perovskites. Ion mobility adds further complexity to the structure, where iodide ions have been shown to play a key role, but no definitive mechanism has emerged [6]. Mobility of all three ions, Pb, I and MA, have been extensively studied [7-10], but, as yet, no definitive mechanism has emerged, although iodide ions have been shown to play a key role [11]. The complex structural features and intrinsic disorder explains the large number of anomalies in the literature as to the exact symmetry and structural parameters [12], which is suggestive of localized symmetry variations that is prevalent in solid electrolytes.

We show that iodide ions migrate through an interstitial (I3) position. This migration is only possible through a correlated rearrangement of the MA ions. Furthermore, a substantial local static distortion of the Pb–I octahedra into a pseudocubic arrangement produces I–I bond distances consistent with the formation neutral I_2 defects that could effectively act as electron/hole pairs.

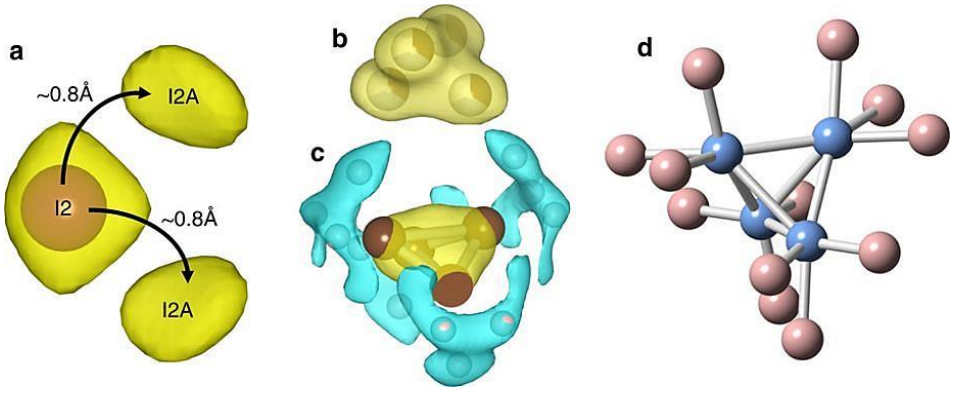

Figure 1. (a) Section of the (100) projection of the nuclear scattering density (yellow) at room temperature (isosurface level of 0.8 fmÅ−3) showing main iodide position (I2, purple sphere) is accompanied by two additional scattering densities (labelled I2A). (b) X-ray scattering and (c) nuclear scattering density map of methylammonium molecules (isosurface level of 1.0 fmÅ−3), showing C and N (yellow) and hydrogen scattering (blue) (d) molecular structure extracted from the maxima in the scattering density maps.

The maximum entropy method (MEM) is an analysis technique that can be applied to diffraction data that generates density maps without prior knowledge of symmetry and unit cell content, and therefore unbiased towards any specific structural model. It can provide information on subtle local distortions even when this scattering is extremely weak compared to the bulk diffraction [13,14].

To gain a deeper insight into the structure of MAPbI we have performed both powder neutron, single crystal X-ray diffraction, and powder synchrotron X-ray studies. The structure was solved in I4/m space group with lattice parameters of a=8.8756(1) Å and c=12.6517(3) Å. The I4/m symmetry is not an isomorphic subgroup of the high temperature cubic perovskite space group, so not a common perovskite symmetry18. However, in the case of MAPbI the transition from cubic to tetragonal is first order, so multiple irreducible representations can be adopted. The principal features of the MAPbI structure derived from the MEM analysis was found to be considerably more complex than previous realized (Fig. 1). The nuclear scattering density around the iodide ion at the (−0.2148(3) −0.2851(3) 0.5) position (I2) at room temperature was found to be localized with typical levels of thermal distribution (Fig. 1a). However, additional densities with similarly localized scattering were identified at two positions in close proximity, demonstrating static disorder of the I2 site, labelled I2A. These were determined to be at (−0.252(3) −0.248(3) 0.453) in a pseudocubic arrangement, and represent a ∼0.8 Å shift from the known I2 position towards the MA ions and lying on either side of a mirror plane in the tetragonal space group. The MEM density maps surrounding the MA ion for single crystal X-ray and powder neutron diffraction showed similar scattering for the C–N that is best described as a 4 atom tetrahedron unit.

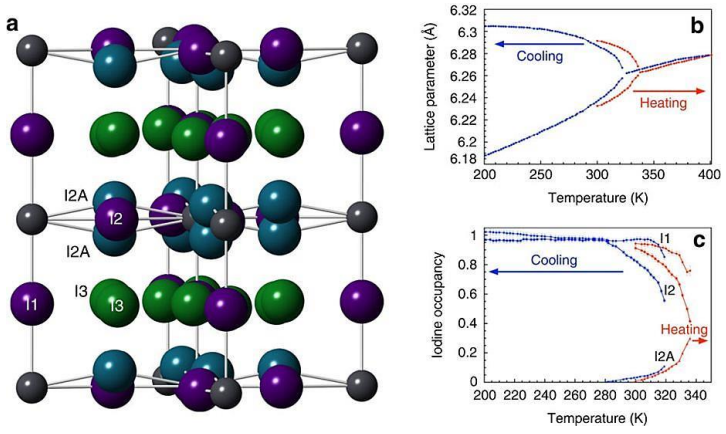

Figure 2. (a) Lead (grey spheres) and iodide positions in the room temperature I4/m space group, showing four crystallographically inequivalent iodide positions within the unit cell at position I1 and I2 (purple) that form the regular perovskite PbI6 corner shared octahedra and two additional position I2A (blue sphere) and I3 (green sphere). The methylammonium ions are omitted for clarity. Powder synchrotron X-ray data shows (b) hysteresis in tetragonal to cubic phase transition, and (c) temperature dependence of the I1, I2 and I2A iodide ion site occupancy as a function of temperature.

A further iodide position (I3) was observed in the powder neutron diffraction, powder synchrotron diffraction and single crystal X-ray diffraction that sits in an interstitial site

in the z~0.25 plane with Pb and MA ions (Fig. 2a). This 15 K variation is mirrored in the composition variation (Fig. 2c) where the I1, I2 and I2A sites were similarly shifted. There was a slight drop in the composition of I1 sites close to the transition to the cubic phase, but the largest variation was in the occupancies of the I2 and I2A ions, where a substantial drop in I2 composition was observed with increases in I2A, but not to the same extent. The I3 content was difficult to accurately determine with the short runs of the synchrotron measurements. However, the total composition was seen to drop slightly, implying the I3 site were being populated, but were diffuse and thereby not contributing to the Bragg scattering to the same extent as the other iodide ions.

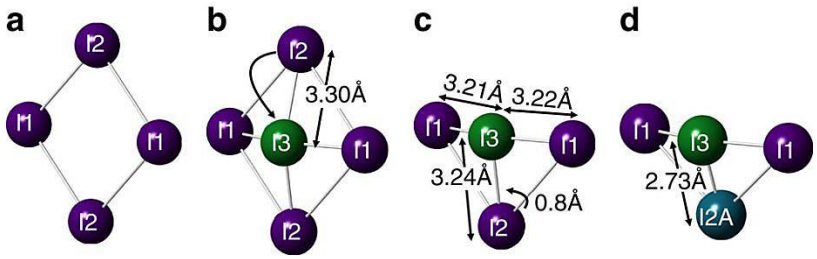

Figure 4. (a) Section of the perovskite structure showing two I1 and two I2 position lying in the plane, (b) Iodine I2 moves to the interstitial I3 position leaving (c) I3 surrounded by three roughly equidistant iodine ions, provoking I2 ions to jump to a I2A position creating (d) bond formation to produce I2 molecules.

From the isolation of these atomic positions and variation of compositions, one can propose a mechanism for ion migration within the cell. The significant drop in composition of the I2 site at temperatures above 280 K, compared with the increased occupancy of the I2A site, implies that I2 are both populating the ion interstitial site, I3, and well as shifting to the new I2A locations. A I2 to I3 hop (Fig. 3a–c) would leave the I3 ions surrounded by three iodide ions all approximately 3.2 Å apart. Given the concomitant increase in the population of the both the I2A and I3 sites over the same temperature regime, the nature of the bonding between these two positions is important. Polyiodide ions are well known to the form multiple low valent iodide chains, where the I–I bond lengths are extremely sensitive to the nature of the bonding and charges on the iodine [15]. Structure of solid I2 is an orthorhombic zig-zag structure with intramolecular I–I bond lengths of 2.68 Å, and intermolecular I2 distances of 3.56 Å (ref. 24). I2 confined within frameworks have similar bond lengths, such as iodine in formate, Zn3(HCOO)6, has a bond length of 2.691 Å with a second weakly interacting molecule at 3.59 Å [16]. The two I3–I2A bond lengths in MAPbI are at 2.7(1) Å and 2.6(1) Å, so from these structural considerations it is consistent with the static disorder and shift from I2 to I2A is the result of covalent I2 bond formation in MAPbI to produce a neutral diatomic I2 molecule within the perovskite framework. This would have extensive implications on the band structure and charge transfer suggests a redox reaction of $2I^- \rightarrow I_2 + 2e^-$. The bond distances between I3 and both orientations of the MA ions are unphysical, which suggests that the occupancy of I3 can only be achieved with the MA molecule adopting a perpendicular orientation (Fig. 4b), such that diffusion of the I3 ions from I2 and I1 only occurs with collective motion of the MA ions in a gate opening type mechanism.

Further studies will be needed to clarify the presence and role of the I2/I− redox couple and the implied electron/hole formation within hybrid perovskite, as well as the effect on the electronic and ionic conduction and whether this is related to its solar conversion properties, such as the long electron-hole diffusion lengths [11] and lifetimes [12].

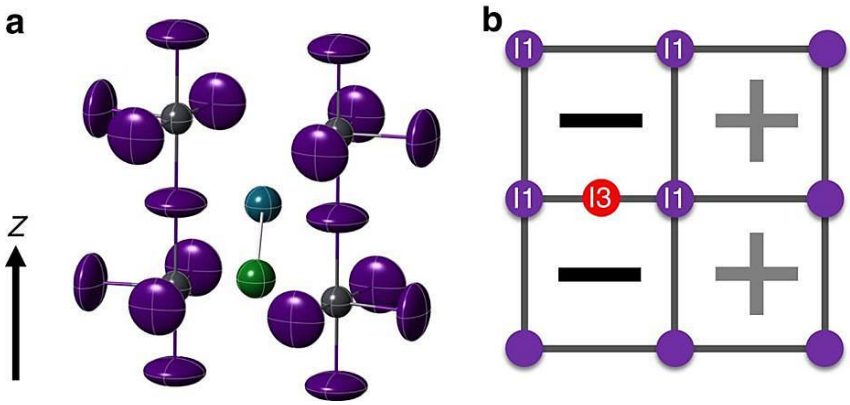

Figure 5. (a) Relative positions of I2 molecule (green and blue sphere) compared to the perovskite framework. Methylammonium ions are omitted for clarity, and (b) cooperative arrangements of the orientation of the methylammonium ions as a result of occupation of I3 sites. (−) and (+) represents single and shared orientations of MA molecule, respectively.

References

[1] Kojima, A., Teshima, K., Shirai, Y. & Miyasaka, J. Am. Chem. Soc. 131, 6050 (2009).
[2] E. Rytter, N.E. Tsakoumis, A. Holmen, Catal. Today 261 (2016) 3–16.
[2] Im, J. H., Lee, C. R., Lee, J. W., Park, S. W. & Park, N. G. Nanoscale 3, 4088 (2011).
[3] Lee, M. M. et al. J. Science 338, 643 (2012).
[4] Kim, H. S. et al. Sci. Rep. 2, 591 (2012).
[5] Liu, M. Z., Johnston, M. B. & Snaith, H. J. Nature 501, 395 (2013).
[6] Yang, T. Y., Gregori, G., Pellet, N., Gratzel, M. & Maier, J. Chem. 54, 7905 (2015).
[7] Yuan, Y. & Huang, J. Acc. Chem. Res. 49, 286 (2016).
[8] Eames, C. et al. Nat. Commun. 6, 7497 (2015).
[9] Walsh, A. et al. Chem. 54, 1791–1794 (2015).
[10] Azpiroz, J. M. et al.. Energy Environ. Sci. 8, 2118–2127 (2015).
[11] Yang, T. Y., Gregori, G., Pellet, N., Gratzel, M. & Maier, J. Chem. 54, 7905 (2015).
[12] Baikie, T. et al. J. Mater. Chem. A 1, 5628 (2013).
[13] Zajdel, P. et al., $Fe_{1+x}Te_{1-y}S_y$. J. Am. Chem. Soc. 132, 13000 (2010).
[14] Nakatsuji, S. et al. Science 336, 559 (2012).
[15] Svensson, P. H. & Kloo, L. Chem. Rev. 103, 1649 (2003).
[16] Harris, P. M., Mack, E. & Blake, F. C., J. Am. Chem. Soc. 50, 1583 (1928).
[17] Stranks, S. D. et al. Science 342, 341–344 (2013).
[18] Wehrenfennig, C., Eperon, G. E., Johnston, M. B., Snaith, H. J. & Herz, L. M. Adv. Mater. 26, 1584 (2014).

Publication

J. L. Minns, P. Zajdel, D. Chernyshov, W. van Beek & M. A. Green. *Nat. Commun*. **8**, (2017) 15152.

Very long-lived photogenerated high-spin phase of a multi-stable spin-crossover molecular material

Teresa Delgado[a], Antoine Tissot[b], Laure Guénée[c], Andreas Hauser[a], Francisco Javier Valverde-Muñoz[d], Maksym Seredyuk[d], José Antonio Real*[d], Sébastien Pillet[e], El-Eulmi Bendeif[e] and Céline Besnard*[c]

a. Département de Chimie Physique, Université de Genève, 1211 Genève, Switzerland.
b. Institut des Matériaux Poreux de Paris, FRE 2000 CNRS, Ecole Normale Supérieure, Ecole Supérieure de Physique et de Chimie Industrielle de Paris, PSL Research University, 75005 Paris, France.
c. Laboratoire de Cristallographie, Université de Genève, 1211 Genève, Switzerland.
d. Departament de Química Inorgánica, Institut de Ciència Molecular (ICMol), Universitat de València, Valencia, Spain
e. Université de Lorraine, CNRS, CRM2, Nancy, France

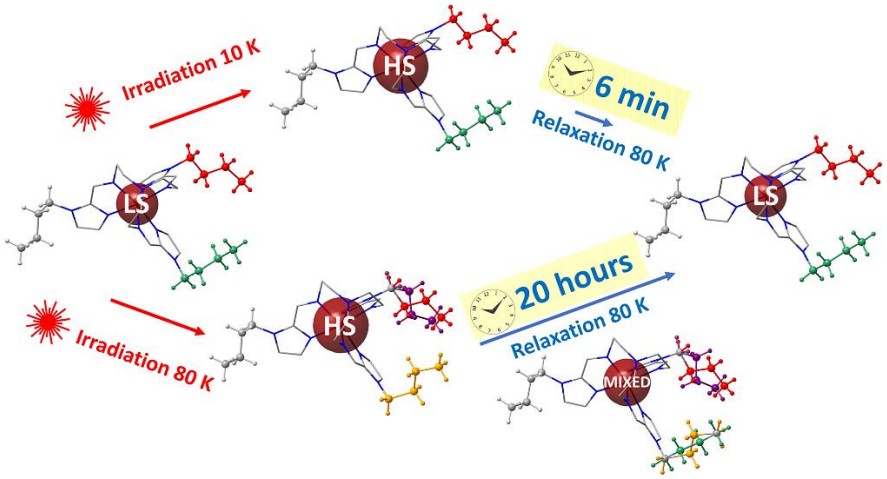

Spin crossover compounds are switchable materials that can be triggered by various external stimuli (temperature, pressure, light and analytes).This makes them good candidates for applications such as spintronic, sensors…[1-2] In the pseudo-octahedral SCO iron(II) complexes, the switch between the HS $t_{2g}^4e_g^2$ and the LS $t_{2g}^6e_g^0$ induces a variation in the Fe-ligand bond lengths that can be as large as 0.2 Å. The spin transition can then be directly followed through the structural changes.

It is possible to achieve a quantitative LS→HS conversion in Fe^{II} SCO complexes by irradiating the sample in the UV-Vis or near-IR regions at low temperature through the "Light-Induced Excited Spin State Trapping" (LIESST) effect [3]. The lifetime of the photogenerated metastable HS state is inversely proportional to the thermal SCO temperature, $T_{1/2}$, at which the molar HS and LS fractions are equal to 0.5. The kinetic stability of the photogenerated HS state can be roughly estimated following a precise protocol which determines the characteristic temperature T_{LIESST} at which the photogenerated HS state relaxes to the LS state within a few minutes after irradiation at 10K [4]. In pure SCO compounds T_{LIESST} values are usually in the interval 20 - 100 K.

$[Fe(n\text{-}Bu\text{-}im)_3tren](PF_6)_2$, (n-Bu-im)$_3$(tren) = n-butyl imidazoltris(2-ethylamino)amine) has a complex spin crossover behavior previously studied by magnetic measurements [5]. Two different thermal spin transitions have been observed depending on the sweeping rate of the temperature. At 4 K/min, the SCO between

the HS and the LS phase (called **LS_1**) is characterized by an average critical temperature of 122 K with a hysteresis loop of 14 K, while for a slower scan rate of 0.1 K/min the SCO between the HS phase and a different LS phase (called **LS_2**) is characterized by an average critical temperature of 156 K and a hysteresis loop of 41 K. Besides the usual HS to LS FeN_6 coordination sphere rearrangements, the HS and LS_1 structures only differ by moderate structural modifications. The HS and LS_2 structures, on the other hand, strongly differ from each other in the orientation of several butyl groups and of the counter anions

We investigated the LIESST behavior of this compounds using absorption spectroscopy and magnetometry. As expected, the HS→LS relaxation after irradiation of the LS_2 phase (irradiation at 10 K) is faster than the HS→LS relaxation after irradiation of the LS_1 phase (irradiation at 10 K). However, during our measurements, we noticed an unusual behaviour for the LS1 phase. Irradiations at temperatures above 70 K of the LS_1 phase lead to unexpected long HS→LS_1 relaxation times as shown in Figure 1. This was not observed for the LS2 phase for which irradiating at higher temperature does not significantly change the relaxation time for a given relaxation temperature.

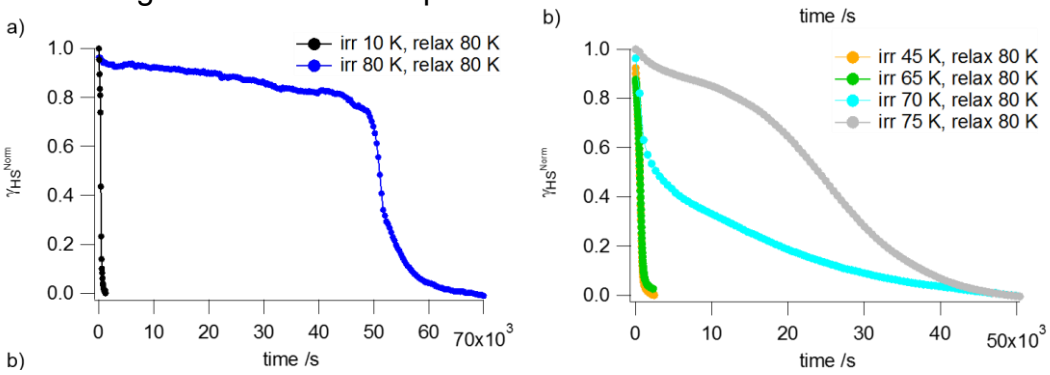

Figure 1. Evolution of the normalized photo-induced HS fraction as a function of time at 80K for the HS to LS_1 relaxation after irradiation of the LS_1 phase at various temperatures. a) Optical spectroscopy data b) Magnetic data. All the experiments start from a quantitative population of the HS state by irradiation at the indicated temperature followed by a relaxation at 80 K

In order to understand the different relaxation behaviors for the LIESST HS state generated below and above 70 K from the LS_1 phase, structural investigations were performed using single crystal X-ray diffraction. The butyl chains of the ligands, which adopt different conformations in the already characterized LS_1, LS_2 and HS states, were closely examined.

A LS_1 structure was obtained at 25 K, which is similar to the one reported at 110 K. After irradiation of the sample, HS structure of the irradiated sample at 25 K, which we will call **HS_1^{1irr}**, presented a complete ordering of all the alkyl substituents, in the same conformation as in the LS_1 state. Around 90 K, the LS_1 structure is similar to the one determined at 25 K. However, the metastable HS excited state that we will call **HS_1^{2irr}** is different, with one of the butyl chains disordered and another butyl chain in a different conformation compared to the structure of LS_1 or HS_1^{1irr}. We were able to collect several datasets during the relaxation. The obtained structures are shown in Figure 2 alongside with the relaxation curve, calculated from the Fe-N distances. In the photoinduced HS_1^{2irr} state, the butyl chain of one ligand is disordered (chain A) with two randomly distributed orientations (red and violet chains). The other butyl

chains (B and C) are ordered. After cutting off the laser irradiation, the relaxation proceeds very slowly for approximately 1 h. During this nucleation time, disorder grows on chain B (green and orange chains). As the relaxation becomes faster, chain A orders in one of its initial orientations (red). Chain B also starts to order, flipping its initial orientation (from the initial orange chain to the final green one). Clearly, this order/disorder phase transition that takes place in two different butyl groups of the ligands is directly related with the long relaxation time.

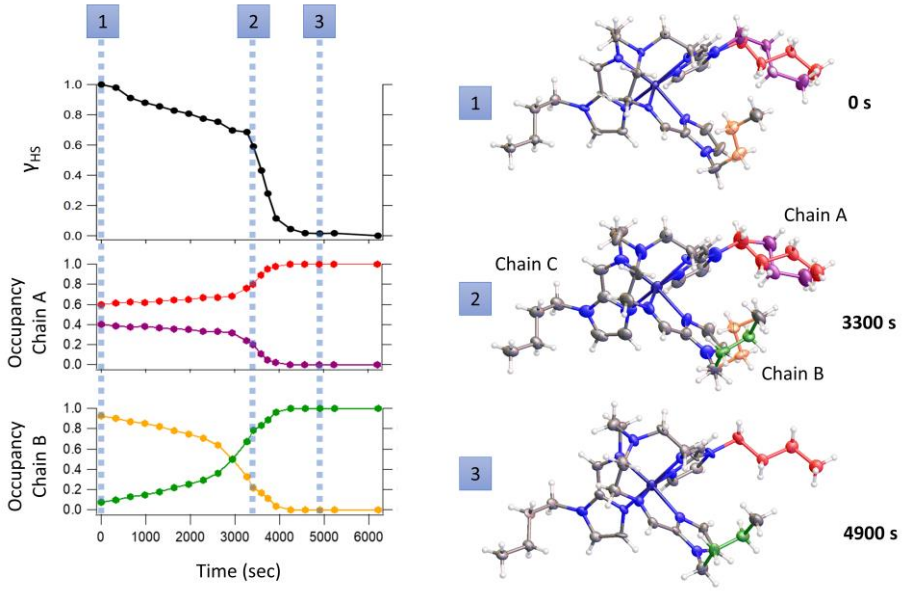

Figure 2. Relaxation curve obtained by single crystal X-ray diffraction using synchrotron radiation at 90 K after irradiation at the same temperature of the LS_1 phase. The HS fraction curve (black) is derived from the crystallographic Fe-N distances. The structure of the complex is shown at three different relaxation times on this curve, with displacement ellipsoids depicted at 40 percent probability level. An order/disorder phase transition takes place in two different butyl groups of the ligand, chain A and B during the relaxation from HS_1^{1irr} to LS_1. For each chain, two different positions of the butyl group are observed, represented with different colors. The occupancy factor defines the proportion of the chain being in the given position. The evolutions with time of the occupancy factors for chain A and chain B are shown below the relaxation curve.

In Figure 3, a structural diagram of the different HS and LS states is presented. This system is a very nice example of how multistability can influence the spin crossover properties. Obtaining long relaxation times at higher temperature is a necessary step for practical applications of spin crossover compounds. A lot of work has therefore been dedicated to increase the so-called T_{LIESST}. Our compound has a T_{LIESST} of 80 K, which is quite low, while the best designed systems are reaching T_{LIESST} of 130 K [6]. However, by using the multistability of the system, we obtained long relaxation times of the order of a few hours at temperatures higher than the T_{LIESST}, by irradiation at temperatures above 70 K. Following the structural changes during the relaxation was a key to understand the LIESST behavior of this system since we could show that this phenomenon can be explained by the rearrangements of side alkyl chains, far away from the spin crossover centres. Multistability is not so rare in spin crossover compounds and this shows that it can indeed be exploited to design systems with interesting photo-induced behaviours.

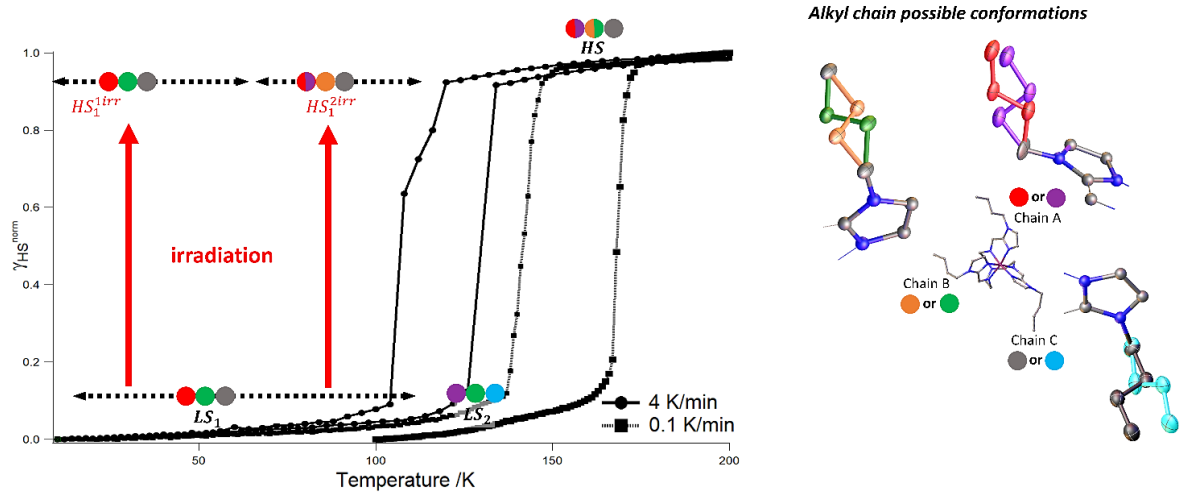

Figure 3. Simplified structural diagram of [Fe(n-Bu-im)$_3$tren](PF$_6$)$_2$; (n-Bu-im)$_3$(tren) = n-butyl imidazoltris(2-ethylamino)amine). The different conformations that the alkyl chains can adopt are shown on the right. For each phase of the phase diagram, three colored disks indicate the positions adopted by chain A, B and C. Two-colored disks indicate that the chain is disordered over both positions. For the quenched phases, a small disorder on chain B is sometimes observed, depending on the temperature, but only the main conformation of the chain has been indicated.

References

[1] Guetlich, P.; Goodwin, H. A.; Editors, *Spin Crossover in Transition Metal Compounds I. [In: Top. Curr. Chem.; 2004, 233]*. Springer-Verlag: 2004;

[2] Halcrow, M. A.; Editor, *Spin-crossover materials: properties and applications*. John Wiley & Sons Ltd.: 2013; p 546 pp.

[3] 15. Decurtins, S.; Guetlich, P.; Koehler, C. P.; Spiering, H.; Hauser, A., *Chem. Phys. Lett.* 1984, *105* (1), 1-4.

[4] Letard, J.-F., *J. Mater. Chem.* 2006, *16* (26), 2550-2559.

[5] Seredyuk, M.; Muñoz, M. C.; Castro, M.; Romero-Morcillo, T.; Gaspar, A. B.; Real, J. A., *Chem. Eur. J.* 2013, *19* (21), 6591-6596.

[6] (1) Hayami, S.; Gu, Z.; Einaga, Y.; Kobayasi, Y.; Ishikawa, Y.; Yamada, Y.; Fujishima, A.; Sato, O. *Inorg. Chem.* **2001**, *40* (13), 3240–3242.

Publication

Delgado, T.; Tissot, A.; Guénée, L.; Hauser, A.; Valverde-Muñoz, F. J.; Seredyuk, M.; Real, J. A.; Pillet, S.; Bendeif, E.-E.; Besnard, C. Very Long-Lived Photogenerated High-Spin Phase of a Multistable Spin-Crossover Molecular Material. *J. Am. Chem. Soc.* **2018**, *140* (40), 12870–12876. https://doi.org/10.1021/jacs.8b06042.

Effect of the active-site structure on the activity of copper mordenite in the conversion of methane into methanol

V. L. Sushkevich[a], D. Palagin[a] and J. A. van Bokhoven[a,b]

(a) Paul Scherrer Institut, Villigen (Switzerland)
(b) Institute for Chemical and Bioengineering, ETH Zurich (Switzerland)

Materials with monomeric and oligomeric copper sites that are active in the direct conversion of methane into methanol possess different reactivity towards methane and water. Here, it is shown for the first time that oligomeric copper species exhibit high activity under both aerobic and anaerobic activation conditions, whereas monomeric copper sites produce methanol only in aerobic processes.

The direct conversion of methane into methanol is an important process industrially, as it provides a sustainable route from an abundant and clean component of natural gas to one of the main precursors for the synthesis of chemicals. A promising aerobic stepwise process over copper-exchanged zeolites has been suggested; however, a detailed understanding of the mechanism of such a zeolite-catalysed conversion is still missing [1, 2].

It has recently been shown that selective anaerobic oxidation of methane is possible [3]; where water is used both to provide oxygen to regenerate the zeolite active sites and to stabilise reaction intermediates to drive the otherwise endothermic Cu^{I} oxidation reaction. Instead of using oxygen, only the presence of water is required, while the reactivation of the zeolite material is done in an inert atmosphere. Such a water-facilitated redox process requires at least two copper atoms to stoichiometrically oxidise methane into methanol, thus suggesting the presence of active sites containing several copper atoms. However, the intrinsic activity of copper species of different sizes is still a subject of debate.

This work demonstrates the influence of the Si/Al ratio of the zeolite mordenite on the possible configurations of the active copper oxide sites, and therefore on the activity of the material in the process of aerobic and anaerobic conversion of methane into methanol. Infrared spectroscopy of probe molecules (nitrogen monoxide and hydrogen) indicated the dominant formation of copper monomeric species for the samples with a high Si/Al ratio, in contrast to the samples with Si/Al ratio higher than 10, where a mixture of copper sites with different nuclearity was detected. Laboratory tests showed the gradual increase of the selectivity and methanol yield per mole of copper with an increase of the Si/Al ratio, which might be associated with different redox properties. To assess them, a temperature-programmed reaction (TPR) of copper mordenite samples with methane was monitored by means of *in-situ* X-ray absorption spectroscopy (XAS) at beamline **BM31**. Cu K-edge X-ray absorption near edge structure (XANES) spectra showed the gradual conversion of Cu^{II} species into Cu^{I} within the temperature range of 300-700 K (Figure 1a). Linear combination fitting (LCF) analysis of the spectra acquired for different samples (Figure 2b) demonstrated that the reduction of all samples starts at ~400 K and then progressively accelerates with the rise of temperature. CuMOR(6.5) and CuMOR(10) demonstrated similar redox properties, with almost full reduction of Cu^{II} into Cu^{I} at 650 K. In contrast, the reduction of the CuMOR(46) material showed a more gradual reduction until the

temperature of 750 K. This indicates lower reactivity of copper monomeric species of CuMOR(46) towards methane.

Combining XAS and infrared spectroscopy with reactor tests, it is possible to show that monomeric and oligomeric copper species display different activities towards methane in both aerobic and anaerobic pathways, as well as towards water under anaerobic conditions. This difference is probably related to the stabilising effect of the water molecules interacting with active copper sites. Together, the data can serve as a basis for the further improvement of existing systems and the design of novel materials for the direct conversion of methane into methanol.

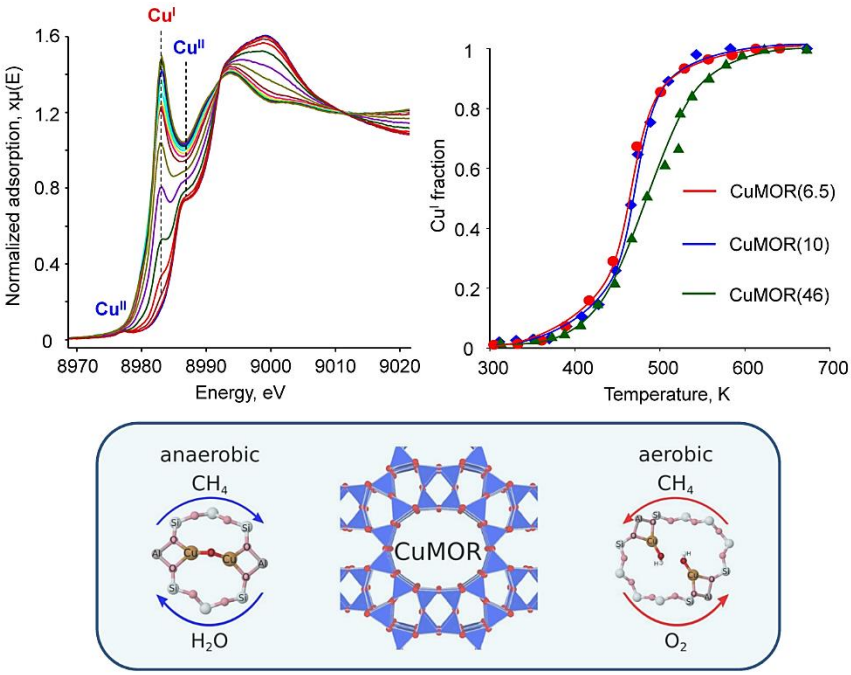

Figure 1: a) Cu K-edge XANES spectra acquired during TPR of CuMOR(Si/Al = 6.5) with methane. b) Results of linear combination fitting of XANES results in the course of TPR-CH_4. c) Scheme representing the aerobic and anaerobic looping protocols for methane conversion into methanol. (*Ed. Panels to be labelled by typesetter. a) top left, b) top right, c) bottom*)

Principal publication and authors

The Effect of the Active-Site Structure on the Activity of Copper Mordenite in Aerobic and Anaerobic Conversion of Methane into Methanol, V. L. Sushkevich (a), D. Palagin (a) and J. A. van Bokhoven (a, b), *Angew. Chem. Int. Ed*., **57**, 8906–8910 (2018), doi: 10.1002/anie.201802922.
(a) Paul Scherrer Institut, Villigen (Switzerland)
(b) Institute for Chemical and Bioengineering, ETH Zurich (Switzerland)

References

[1] M. H. Groothaert *et al., J. Am. Chem. Soc*. **127**, 1394–1395 (2005).
[2] P. Tomkins *et al., Acc. Chem. Res*. **50**, 418–425 (2017).
[3] V. L. Sushkevich *et al., Science* **356**, 523–527 (2017).

STATUS OF FACILITY

BM01

BM01 is a general crystallography beamline focused on diffraction experiments with powder, single crystal, and thin film samples [Dyadkin, V et al. J. Synchrotron Rad., 23, 3, 2016]. We offer a goniometry that hosts a variety of sample environment cells to control temperature, pressure, gas atmosphere, electric and magnetic field at the sample position. The diffraction signal is detected by a hybrid pixel Pilatus2M 2D-detector. A flexible detector support allows to combine experiments covering large scattering angle range with high angular resolution measurements. The diffractometer is controlled by home-developed software “Pylatus”, a set of data processing and data analysis tools developed at SNBL helps users to process, visualize and pre-analyse data during the experiment (for recent updates see https://soft.snbl.eu).

In 2017-2018 BM01 has continued its successful operation and stays one of the most requested and productive crystallography and diffraction station at ESRF.

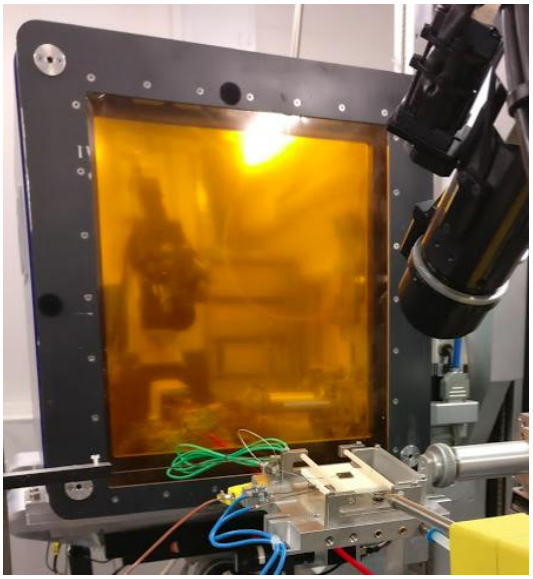

Figure 1. PILATUS@SNBL diffractometer set for in-situ thin film measurements (experiment 01-02-1176, EPFL LNCE, Sion, Switzerland)

The ESRF upgrade will replace existing bending magnet with a 2 pole wiggler source. The existing optics has to be modified in order to handle higher thermal load and to get more from the new source. We have started an upgrade with replacement

of the existing monochromator with a new version of double crystal focusing device designed and constructed by the IDT company. The new monochromator was installed and commissioned in March 2018 (Fig. 4) during service time, without any perturbation of beamline operations and without any user experiment cancelled for this upgrade.

Figure 2. Installation of the new monochromator in the optic hutch of BM01.

Scientific results

2017 and 2018 were very productive years for BM01 with over 140 publications. The publications cover a broad range of topics in modern physics, chemistry, and material science. Many of them have been done in a cross-border collaboration between different research groups. Here we give only a brief overview of selected publications, a complete list can be found at http://www.snbl.eu .

Diffraction data collected at BM01 were combined with neutron scattering data and together revealed a spiral spin-liquid in $MnSc_2S_4$ [Gao, S et al. *Nature Physics*, **13**, 157-161, 2017] and a manifold of magnetic ordered states in $MgCr_2O_4$ [Gao, S et al. *Phys. Rev. B* **97**, 134430, 2018]; the both publications originate from PSI and may serve as an example of a successful single crystal synchrotron experiment at helium temperatures. Another example of crystallography at low temperatures is given by a contribution from the University of Bergen [Bernhardt, P.V et al *Chem. - A European J.*, **24**, 5082, 2018] where temperature evolution of spin state of a Fe^{2+} complex and conjugated structural distortions has been followed in details.

A control of physical properties and crystal structures of photo-switchable materials was in the focus of experiments done by scientists from University of Geneva [Perez, M.T.D. et al. *J. Am. Chem. Soc*., in press, 2018], [Delgado, T. et al. *Phys. Chem. Chem. Phys*., **20**, 12493, 2018], and EPFL [Glushkova, A. et al. *CrystEngComm*, **20**, 3543, 2018].

A significant number of in-situ experiments were focused on gas adsorption by porous materials, such as zeolites and metal-organic frameworks (MOFs). Porous framework materials and various applications of them have been studied by

researchers from the University of Bergen [Bezrukov, A. et al. *Inorg. Chem*., **56**, 12830, 2017; Bezrukov, A. et al. *Cryst. Growth Des*.,**17**, 3257, 2017; Pato-Doldán, et al. *ChemSusChem*, **10**, 1710, 2017; Bezrukov, A. *Chem. Commun*., **54**, 2735, 2018] and Sion branch of EPFL [Peng, L et al. *ACS Appl. Mater. Interfaces*, **9**, 23957, 2017; Bulut, S et al. *J. Org. Chem*., **83**, 3806, 2018; Gladysiak, A. et al *Inorg. Chem*., **57**, 1888, 2018; Gladysiak, A *ACS Appl. Mater. Interfaces*, in press, 2018].

Electrochemistry and battery-related research is another hot topic in material science where users of BM01 were active in 2017-2018. Data collected at BM01 have been used in [Duchêne, L. et al. *Energy Environ. Sci*., **10**, 2609, 2017] for characterization of a sodium-ion battery (EMPA and University of Geneva). Another example of battery research is given in [El Kharbachi et al. *RSC Adv*., **8**, 23468, 2018] (Institute for Energy Technology, Kjeller, SINTEF ,Trondheim, and University of Oslo), where a new composite-electrode concept is proposed for Li solid state batteries.

Based on the accurate data collected with small single crystals a few new crystal structures were solved for unprecedentedly large coordination cages [Cecot, G et al. *J. Am. Chem. Soc*., **139**, 8371, 2017] (EPFL). New materials that are potentially interesting for the food industry, ionic co-crystals of sodium chloride with carbohydrates, have been synthesised and their crystal structures have been solved with BM01 data [Oertling, H. et al. *Cryst. Growth Des*., **17**, 262, 2017] (Unviersity of Geneva and Nestlé Research Center), the compounds are regarded as inexpensive, nontoxic, and biodegradable source of sodium and calories.

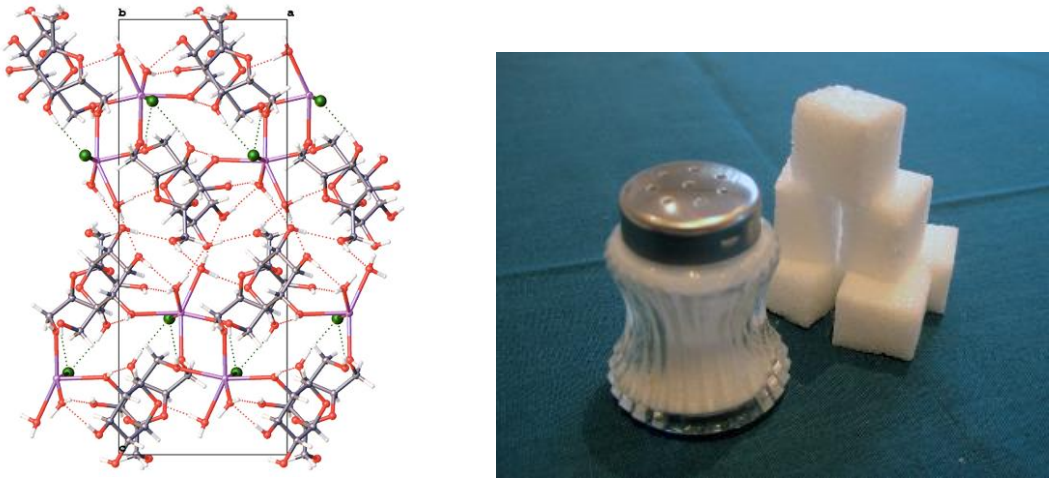

Figure 3. Representation of the crystal structure of sucrose·NaCl·2H_2O. Oxygen atoms are depicted in red, carbon atoms in grey, chlorine atoms in green, sodium atoms in pink, and hydrogen atoms in white, from *Cryst. Growth Des.*, **17**, 262, 2017.

An example of time-resolved powder diffraction experiment is given in an in-situ study of hydrothermal synthesis of $NaNbO_3$ [Skjærvø, S.L et al. *Cryst. Growth Des*., **18**, 770-774, 2018] (NTNU, Tronheim). The high time-resolution (0.1 s) revealed a sequence of transient intermediate phases, including several new phases, before the final perovskite $NaNbO_3$ was formed. These findings highlight the complexity of the hydrothermal synthesis of $NaNbO_3$ and demonstrate the potential for obtaining in-

depth-knowledge of the reactions taking place by time-resolved in-situ X-ray diffraction.

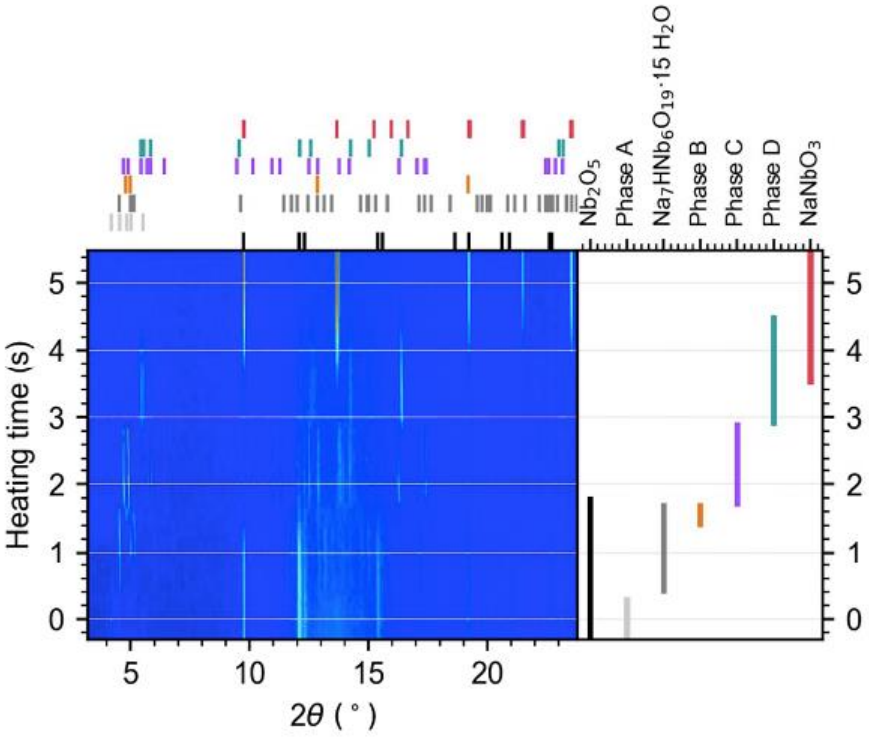

Figure 4. 2D contour plot of the evolution of phases in the Na-Nb-O system for hydrothermal synthesis during rapid heating approaching supercritical conditions (423 °C and 250 bar) including a schematic showing the phase development., from *Cryst. Growth Des*., **18**, 770-774, 2018.

Future developments on the beamline

ESRF is preparing for a major upgrade with the Extremely Brilliant Source (EBS) project. EBS not only offers new opportunities for SNBL beamlines but also changes the source position and in 2019-2020 we have to do a component-by-component re-positioning of the entire beamline. In 2017 we have prepared a 2-phase plane for the development of the both beamlines. For BM01, at the first stage a new monochromator is installed in 2018, and our old mirror system will be refurbished in 2019. We also plan a list of modifications in the experimental hutch to make the future upgrades possible, the modifications include installation of a new beam conditioning and sample positioning unit that integrates a fluorescence detector, optical spectroscopy and microscopy tools, a new fluid distribution panel, a new compact slit vessel, a relocation of the control electronics and diffractometer base.

At the second stage we plan to enhance the single crystal diffraction experiments for fast high quality redundant and complete data acquisition. Millisecond time resolution would be possible with an Eiger X 500k or similar detector, in particular, for a surface

diffraction and in-situ time resolved experiments. Finally, a modified long diffractometer base would allow small-angle scattering experiments using the same detectors.

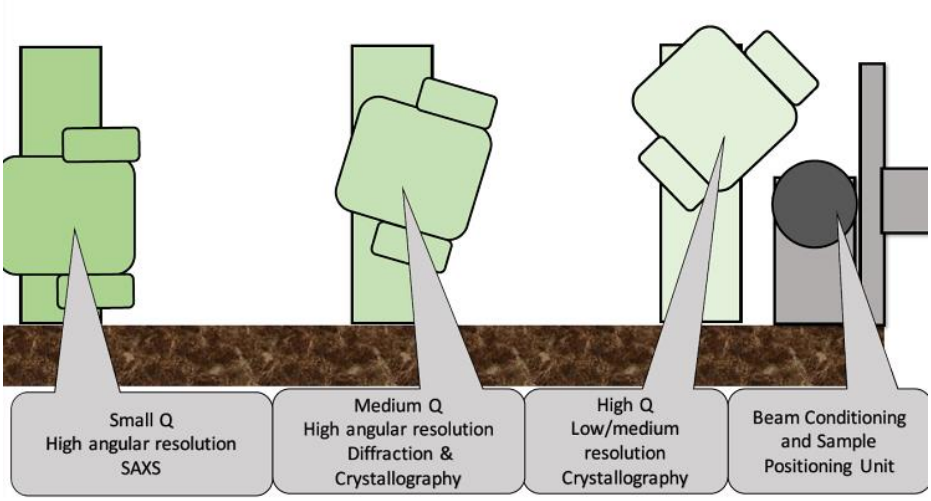

Figure 5. A conceptual scheme of BM01 multipurpose diffraction station, from "SNBL 2019 and 2020: adapt and upgrade the SNBL beamlines to the ESRF Extremely Brilliant Source (EBS)".

BM31

Powder Diffraction and EXAFS Station

Current status

Until 2016 SNBL has been a split beamline, where the x-ray beam emitted from one ESRF bending magnet was subsequently cut into two branches to provide x-rays for two independent end stations: BM01A and BM01B.
Our Swiss and Norwegian funding agencies and the ESRF agreed in June 2014 to move our existing beamline BM01B to a new and independent ESRF bending magnet port: BM31, which, after a two years planning and installation period was successfully completed in 2016 with an effective downtime of 3 month only (see also last status report). The transferred beamline, the new hutches and the newly installed infrastructure have been working flawlessly since the move has been completed 2 years ago.

One of the main arguments for the splitting of the two beamlines were the lack of space i.e. for BM01B due to the vicinity of the A-branch. Moving BM01B to a new bending magnet port held the promise to prepare BM31 for the future, i.e. in the light of the ESRF upgrade, which will start at the end of 2018 and last until summer 2020.
BM31 will seize this occasion to perform radical changes to the existing beamline optics during this shutdown, in line with the declared goal to improve the station performance. This will comprise a new liquid nitrogen cooled monochromator, able to change quickly between different techniques, namely: powder diffraction, EXAFS and Total Scattering. Furthermore the future installation of collimating/focusing mirrors will be prepared in order to collect more photons from the source with the intention to increase the data quality and yet reducing the measurement time. These changes will be reported in more detail in future status reports.
Besides user operation and the planning for the new beamline layout, the BM31 team has equally made new developments which are showing very encouraging results.

Battery research is a rapidly growing field with a high economic and environmental impact. It is thus no surprise that about 20% of the BM31 beam time is now dedicated to this fast moving field of interest.
In the past, BM31 has developed - in collaboration with scientist from the University of Oslo - a standard cell allowing to characterize a plethora of different battery types under different working conditions using X-ray techniques.
The results of this development have been published in the "*Journal of Applied Crystallography*" under the title "*Versatile electrochemical cell for Li/Na-ion batteries and high-throughput setup for combined operando X-ray diffraction and absorption spectroscopy*" (J. Appl. Cryst. (2016) **49**, 1972–1981) and the essence of it has also been shown in the last status report. The recurring request for battery systems working under high temperatures (≦ 100°C) has led to the development of a high temperature sample changer, where up to six battery cells can be mounted in a heat

resistant vermiculite wheel, which allows to sequentially investigate 6 individual cells with our x-ray beam following a user programmed script. Each cell can be set and stabilized at its own user chosen temperature and a connected galvanostat permits for each cell the parallel acquisition of electric data along with the x-ray data. Temperatures can be set as high as 200°C which is also the high end of the working range of our universal battery cell.

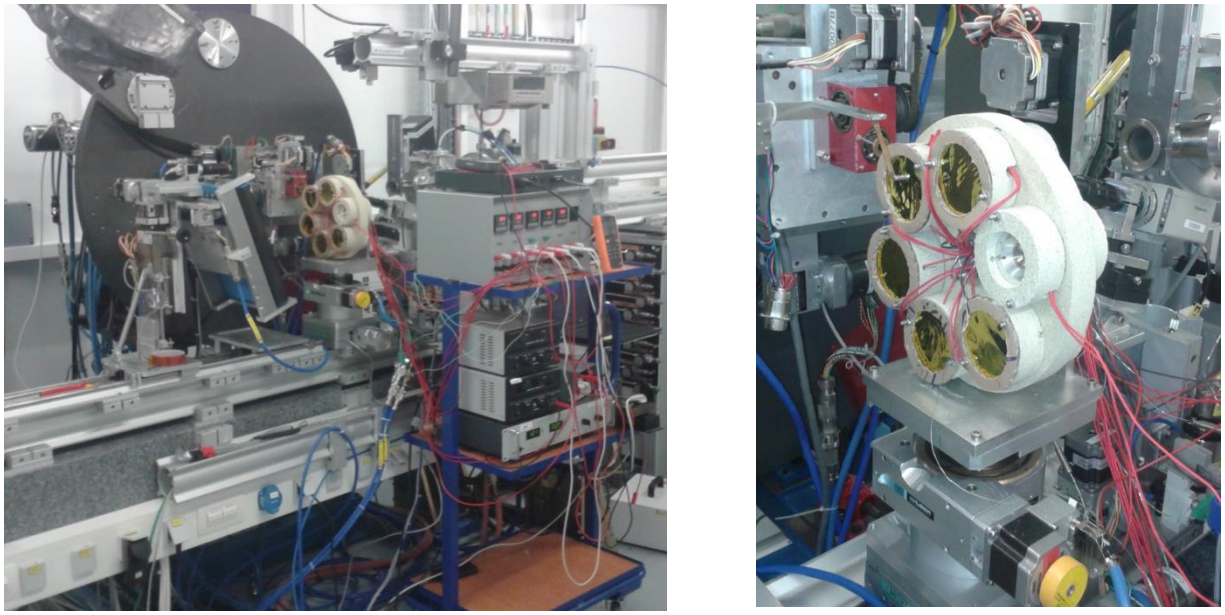

Figure 1. High temperature battery set-up Implementation of the high temperature battery set-up on BM31, showing the inclined Dexela 2D detector, the temperature control unit and the high temperature (HT) wheel (Top). Right: Close-up of the HT sample changer wheel and its connecting cables to the galvanostat.

Driven by the user need and their wish to add fluorescence techniques to our already existing x-ray tool park, a second, new battery cell was developed in 2017 in collaboration with Oleg Drozhzhin et al. (Chemistry Department, Lomonosov Moscow State University) and the SNBL beamline members. This new cell has the advantage to be very easy to assemble which is an important criterion since most of the batteries have to be put together in a glove box under a protective atmosphere. The geometry of the new cell allows to detect the fluorescence photons emitted by the electrode under investigation, which can, in turn, provide important information about the environment of active atoms and their valence state at any moment of the charging/discharging cycles of the cell. The working principle and some relevant measurements showing the potential of this new design have been published in the "*Journal of Synchrotron Radiation*" at the beginning of 2018 under the title: "*An electrochemical cell with sapphire windows for operando synchrotron X-ray powder diffraction and spectroscopy studies of high-power and high voltage electrodes for metal-ion batteries*" (J. Synchrotron Rad. (2018) **25**, 468–472).

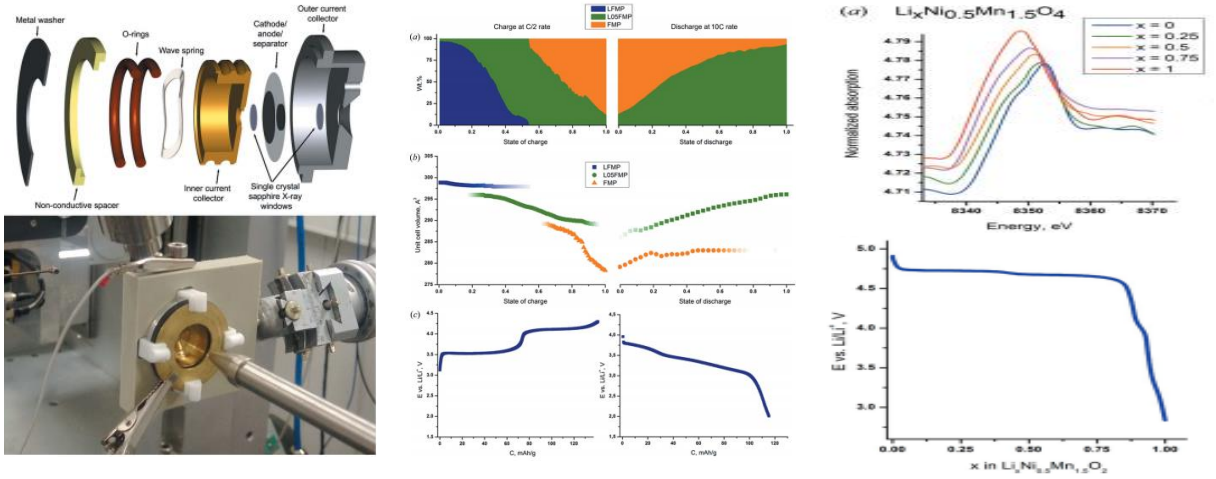

Figure 2. Left top: Exploded view of the new cell, Left bottom: As mounted on BM01 Center: Mass fractions of the developing phases in the Li_1–$xFe_{0.5}Mn_{0.5}PO_4$ positive electrode upon charging/discharging as refined from diffraction data and its respective charge/discharge diagram (Center bottom). Right: XANES from the Ni K-edge and the corresponding discharge curve in the $Li_{1-x}Ni_{0.5}Mn_{1.5}O_4$ cathode material.

New focusing System

The biggest improvement in 2017 has certainly been the installation of a new focusing system for diffraction experiments. Before moving to the new BM31 bending magnet the former SNB station was already equipped with a focusing crystal for energies around 40keV. Compared to an unfocused beam this system allowed for a 7-10fold flux density increase and thus an accordingly reduced measurement time. Due to the beamline move the respective distances from the x-ray source to the monochromator as much as the distance between the monochromator (holding the focusing crystal) and the sample have changed by several meters. Therefore a new focusing crystal had to be ordered and installed towards the end of 2017.
This focusing crystal was produced by bonding a Si 111-oriented wafer onto a Pyrex substrate with a fixed cylindrical radius ground in to the Pyrex block prior to the bonding.

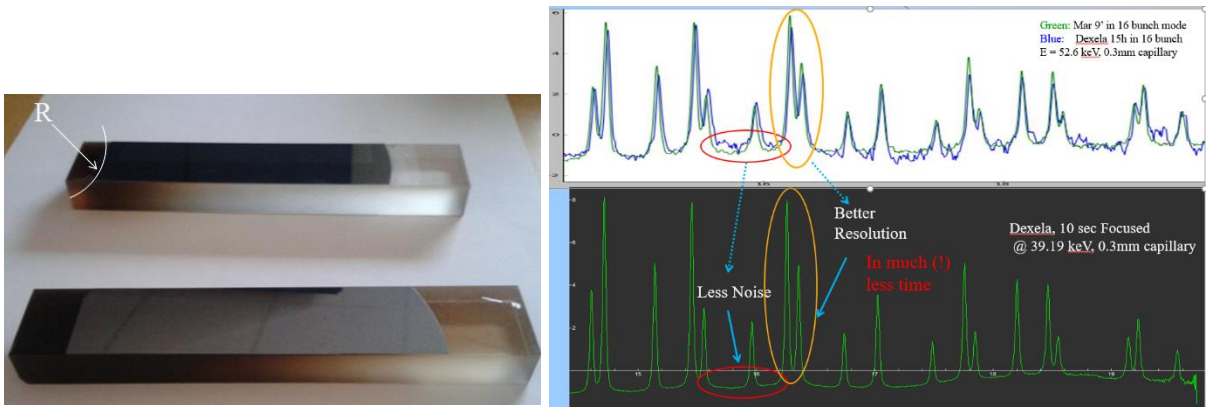

Figure 3. Left: Pyrex support with fixed cylindrical radius (R~1m) ground in and a Si-111 wafer anodically bonded to its surface. Right Top: Diffraction measurements using an unfocused beam on LaB6, done with two different 2D detectors (Mar /Dexela) Exposure time ~ 9 min and 15h (16-Bunch) respectively. Right Bottom: Same sample, measurement done in 10 seconds only, using the focusing device and the Dexela 2D-Detector.

The first results of this new type of focusing are truly impressive. The flux density is estimated to be about 250 times higher compared to an unfocused beam at the same energy (39.2keV). Furthermore the full width half maximum of the focal spot size at the sample position is below 100um. The outcome of this improvement is not only a dramatically reduced measurement time, but equally a substantially enhanced resolution due to the small focal spot size. Furthermore the (thermal) detector noise of our (medical) 2D Dexela detector got largely suppressed, due to the much shorter exposure times. First measurements on samples provided by our users confirm the greatly improved data quality.

Scientific results

After resuming its activities in autumn 2016, BM31 has maintained its productivity in terms of scientific output as it will be illustrated in the following few examples.

BM31 has been streamlined to follow dynamic chemical and physical processes in real time. This holds especially for the quasi simultaneous combination of diffraction techniques probing the long range structural information in ordered samples together with x-ray spectroscopy (XAFS) yielding the short the range order even in amorphous samples. Performing both experiments on the same sample spot allows for a perfect temporal correlation of the information gained by one technique with the results of the measurements obtained by the other.
The strength of this combination can be seen in the publication from C. Andersen, et al. under the title: "*Redox-Driven Migration of Copper Ions in the Cu-CHA (SSZ-13) Zeolite as shown by the In Situ PXRD/XANES Technique*" published in the renowned Journal "Angewandte Chemie" (**56**, 10367–10372, 2017).
Using quasi-simultaneous Powder Diffraction (PD) and XAFS on a commercially available de-NO_x Zeolite catalyst: Cu-CHA, they could track both, the oxidation state of the redox active centers, as well as their structural location and migration in the zeolitic network during the different stages of the catalytic activation.

In this article the experimentalists establish a direct correlation between the reduction of Cu^{2+} to Cu^{+} and the migration from an accessible, but relatively unstable configuration in the 8R of CHA to the less accessible, but more stable configuration in the 6R.
The authors conclude that the reduction process does not begin until all the water has dissipated, and the kinetic energy overcomes a thermal activation energy corresponding to about 400°C and that at least two separate Cu^{+} sites are present in Cu-CHA, expanding the known Cu^{+}-loaded CHA model with an 8R site.
From an experimental point of view the take away message is, that it is really the power of combining in situ PXRD and XANES which permits to monitor simultaneous cation migration and redox chemistry in this dynamically evolving sample.

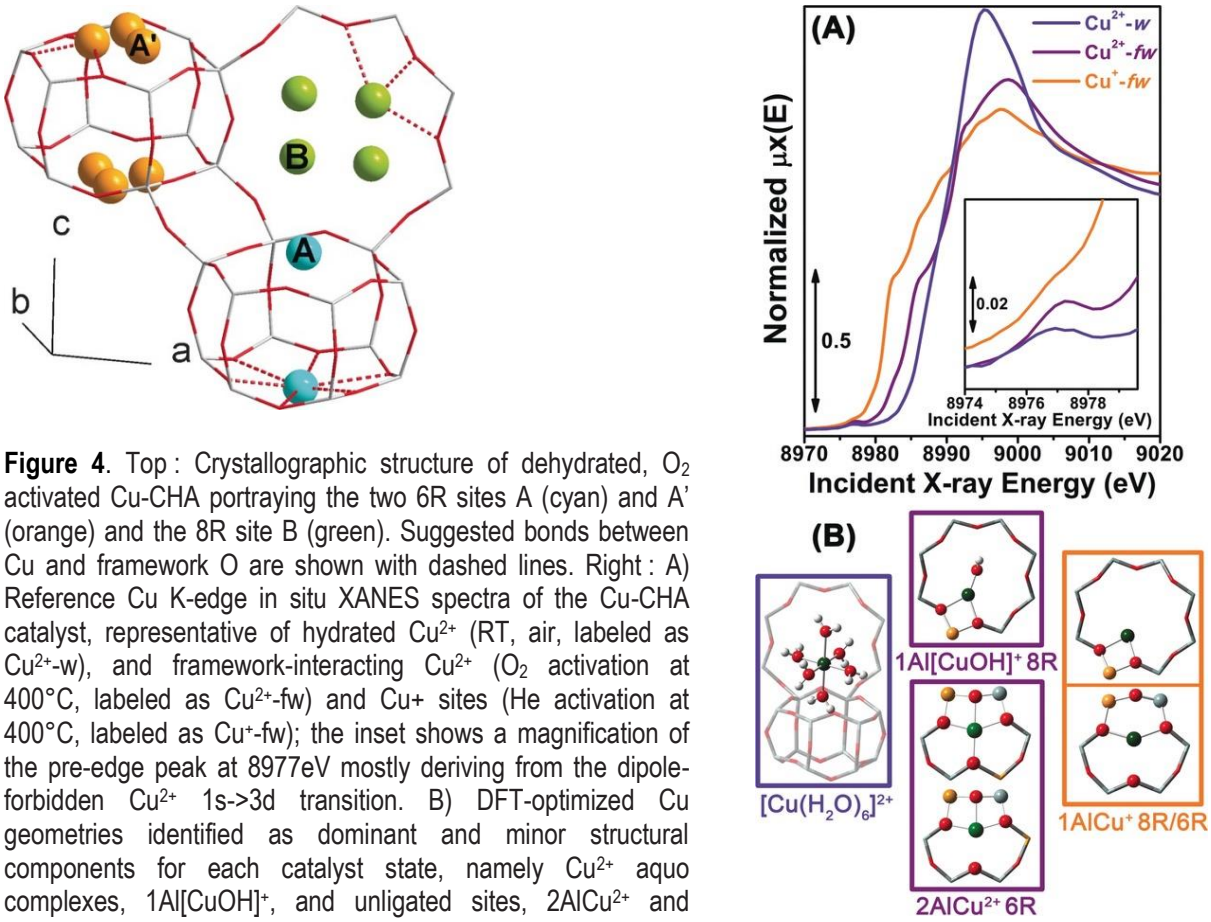

Figure 4. Top : Crystallographic structure of dehydrated, O_2 activated Cu-CHA portraying the two 6R sites A (cyan) and A' (orange) and the 8R site B (green). Suggested bonds between Cu and framework O are shown with dashed lines. Right : A) Reference Cu K-edge in situ XANES spectra of the Cu-CHA catalyst, representative of hydrated Cu^{2+} (RT, air, labeled as Cu^{2+}-w), and framework-interacting Cu^{2+} (O_2 activation at 400°C, labeled as Cu^{2+}-fw) and Cu+ sites (He activation at 400°C, labeled as Cu^{+}-fw); the inset shows a magnification of the pre-edge peak at 8977eV mostly deriving from the dipole-forbidden Cu^{2+} 1s->3d transition. B) DFT-optimized Cu geometries identified as dominant and minor structural components for each catalyst state, namely Cu^{2+} aquo complexes, $1Al[CuOH]^{+}$, and unligated sites, $2AlCu^{2+}$ and $1AlCu^{+}$.Cu green, H white, O red, Si gray, Al yellow

The following example shows the close collaboration between the beamline members and SNBL users. In the article "*In situ flow cell for combined X-ray absorption spectroscopy, X-ray diffraction, and mass spectrometry at high photon energies under solar thermochemical looping conditions*" from Matthäus Rothensteiner *et al*. (Rev. of Scientific Instruments **88**, 083116 (2017). In this article an in situ/operando flow cell for transmission mode X-ray absorption spectroscopy (XAS), X-ray diffraction (XRD), and combined XAS/XRD measurements in a single experiment under the extreme conditions is presented. This cell has been developed by the main author and the beamline scientist of BM31 (H. Emerich). The object of this study was a two-step solar thermochemical looping process for the dissociation of water and/or carbon dioxide. The resulting gases can be reused to form hydrocarbons in the well-known Fischer Tropsch Reaction (FTR).

In this set-up the reaction materials are exposed to the relevant conditions of both, the auto-reduction and the oxidation sub-steps in a thermochemical cycle at ambient temperatures up to 1773 K. The composition of the effluent gases are monitored online by quadrupole mass spectrometry. The cell is based on a tube-in-tube design and is heated by means of a focusing infrared furnace.

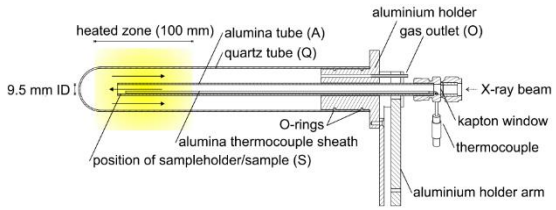

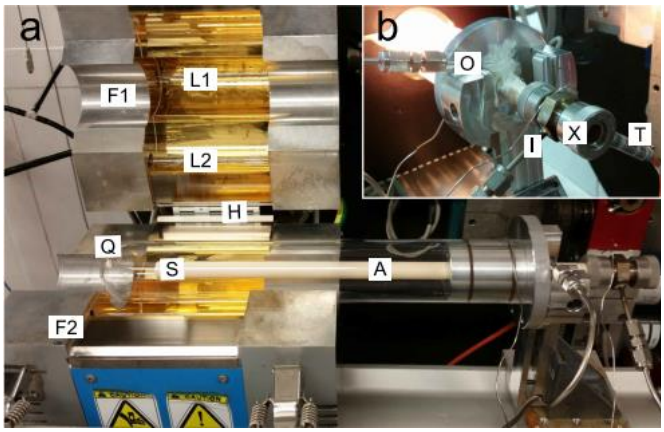

Figure 5. Left: Quartz dome and inner alumina feed-gas/sample container. X-rays enter from the right, the round dome at the end of the furnace allows to collect diffraction patterns over a large angular range. Right: The system mounted in an infrared furnace, allowing to expose the sample to temperatures up to 1773K in a controlled gas in/out flux.

The oxidation state and off-stoichiometry of the thermally active sample ($Ce_{0.5}Hf_{0.5}O_{2-\delta}$, where δ stands for the off-stoichiometry) could be monitored over the full temperature range by the use of Xanes techniques at the Ce and Hf K-edges at 40.4keV and 65.4keV respectively. Structural information (i.e. the formation of a monoclinic Hafnia phase) could be obtained during the thermal looping cycles by the use of powder diffraction in combination with the focusing crystal at ~40keV.

Another example is the research work on sodium batteries done by Jonas Sottmann et al, published in "Chemistry of materials" in 2017. (*Chem. Mater.* 2017, **29**, 2803-2809). Sodium-Ion batteries are prime candidates for energy mass storage due to the abundance of sodium, its low price and low toxicity. In this study, entitled *"Bismuth Vanadate and Molybdate: Stable Alloying Anodes for Sodium-Ion Batteries"* it is shown, that bismuth metalates, $BiVO_4$ and $Bi_2(MoO_4)_3$, chosen as representatives of ternary metalates for anode materials of Na-batteries, show high specific capacities (367 mAh/g and 352 mAh/g, respectively) and exceptionally high cycling stability for alloying anodes with close to 80% of the first charge capacity retained over 1000 cycles at ~1C (in the case of $Bi_2(MoO_4)_3$) and a Coulombic efficiency well above 90% for both materials. Furthermore, $BiVO_4$ is a low cost commercial yellow pigment with low toxicity.
In situ XANES studies on BM31 (using our in-house developed battery cell), ex situ XRD, and DFT analysis suggest that the initial compounds upon first time sodiation are converted into alloying Bi nanocrystallites confined in a matrix of electrochemically active insertion hosts namely $Na_{3+x}VO_4$ and Na_2+xMoO_4 respectively.

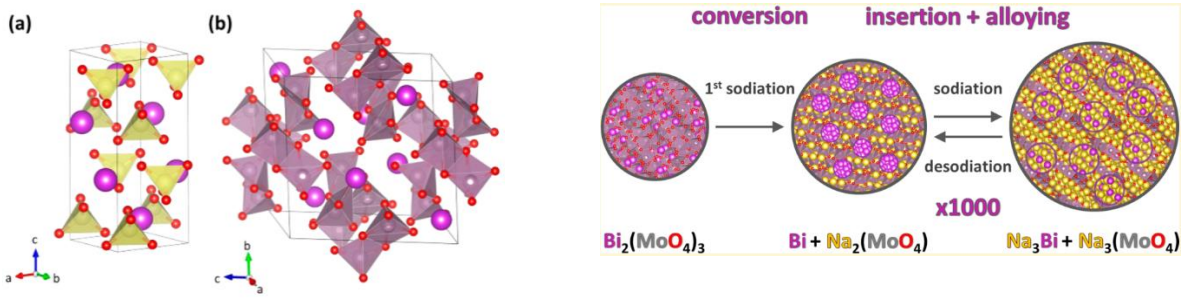

Figure 6. **Left:** Crystal structure of (a) $BiVO_4$ and (b) $Bi_2(MoO_4)_3$. Purple, yellow, grey and red balls represent Bi, V, Mo, and O atoms, respectively. **Right:** (De-)Sodiation pathways. Initial sodiation and initial formation of Na_3VO_4 and Na_2MoO_4 and subsequent charging/discharging cycles.

The formation of an electrochemically active Na_3VO_4 and Na_2MoO_4 matrix after the initial, irreversible conversion of $BiVO_4$ and $Bi_2(MoO_4)_3$, respectively (1^{th} sodiation), is seen as one of the major reasons for the excellent battery performance.

SNBL - FACTS AND FIGURES

BUDGET (in kEUR)

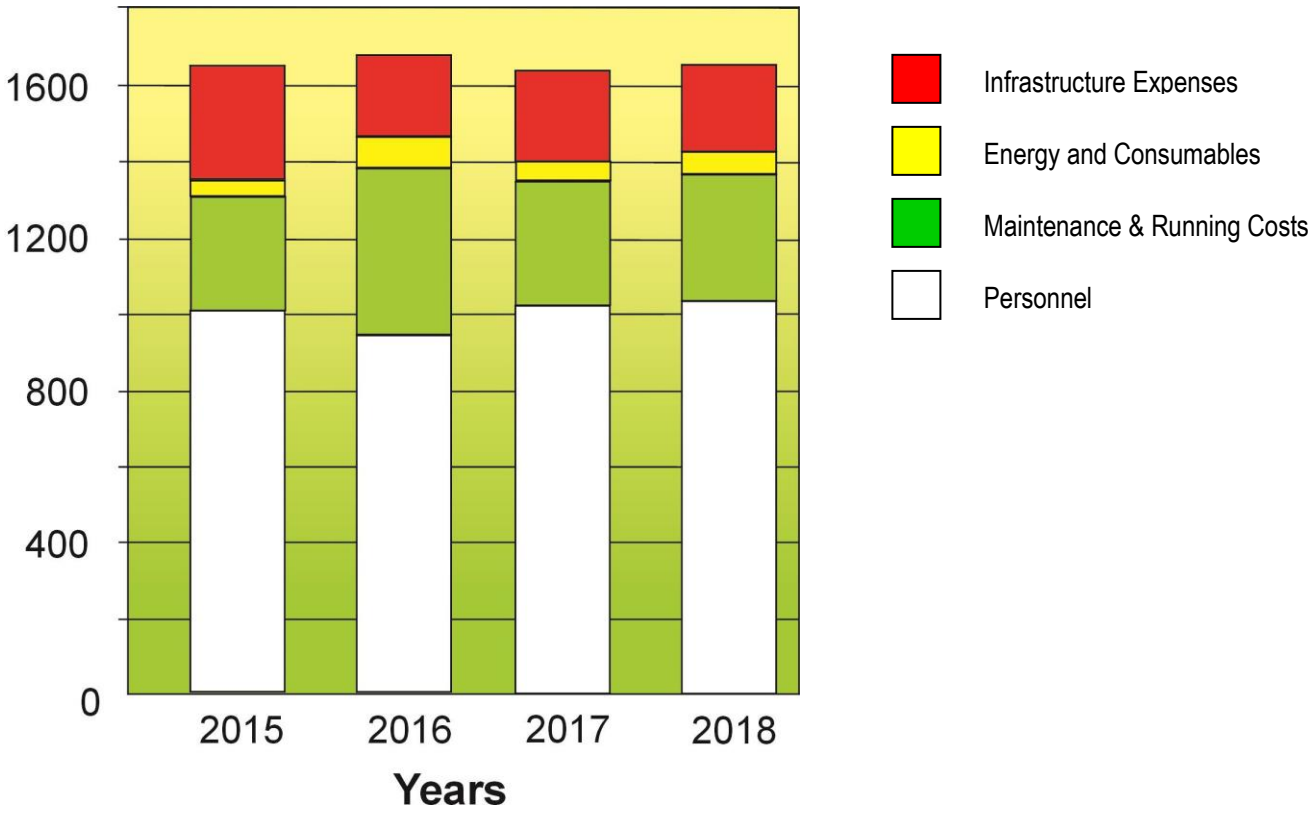

BUDGET in kEUR	2015	2016	2017	2018
Personnel	1,008	965	1,010	1,020
Maintenance and Running Costs	350	423	332	342
Energy and Consumables	48	50	50	50
Infrastructure Expenses	214	222	228	228
TOTAL	**1,620**	**1,660**	**1,620**	**1,640**

INCOME (in kEUR)

Income Outside Contract

Income According to Contract

Miscellaneous Income

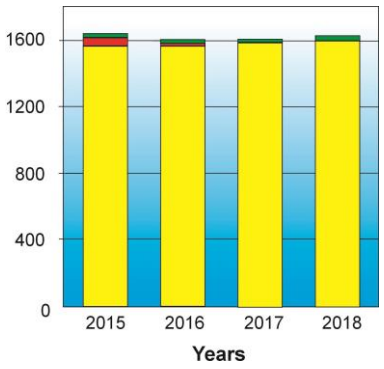

INCOME in kEUR	2015	2016	2017	2018
Income According to Contract	1,560	1,563	1,586	1,628
Income Outside Contract	59	18	-	-
Miscellaneous Income	27	35	13	3
TOTAL	**1,646**	**1,616**	**1,599**	**1,631**

EXPENDITURE (in kEUR)

Infrastructure Expenses

Energy and Consumables

Maintenance & Running Costs

Personnel

BM 01 Upgrade

BM31 Construction

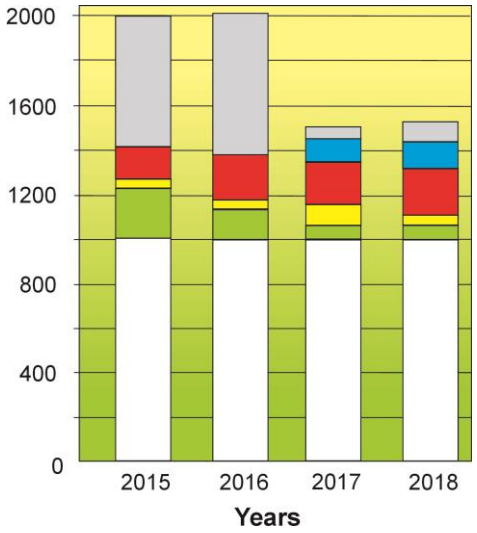

EXPENDITURE in kEUR	2015	2016	2017	2018
Personnel	1,020	1,000	997	1,000
Maintenance and Running Costs	189	142	85	67
Energy and Consumables	37	48	85	53
Infrastructure Expenses	166	184	198	205
BM01 Upgrade			105	134
BM31 Construction	590	684	38	87
TOTAL	**2,001**	**2,058**	**1,509**	**1,546**

Organization Chart of the SNBL

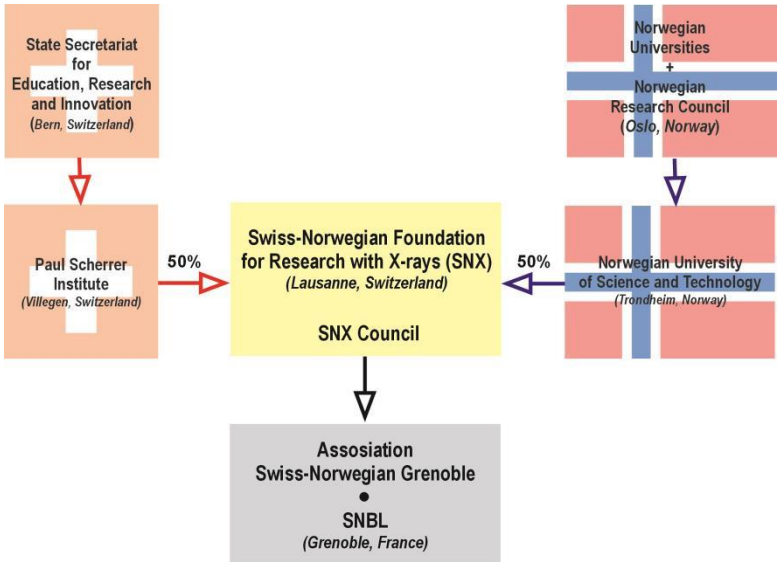

SNX Council

MEMBERS (2018)

Prof.H.Fjellvag– Chairman	University of Oslo, Norway
Prof. G. Chapuis – Vice-Chairman	EPF Lausanne, Switzerland
Prof. M.Ronning	NTNU, Trondheim, Norway
Dr. N.Casati	SLS / PSI, Switzerland
Prof. R.Cerny	University of Geneve, Switzerland
Prof. B.Hauback	IFE, Kjeller, Norway
Dr. V. Dmitriev	SNBL, Grenoble, France

SNBL Staff

(2018)

Dr. V. Dmitriev – Project Director

BM01	*BM31*
Dr. D. Chernyshov – BL responsable	**H. Emerich** – BL responsable
Dr. V.Dyadkin – BL scientist	**Dr. W. van Beek** – BL scientist, deputy director of SNBL
Dr. Iu.Dovgaliuk – BL scientist	**Dr. M.Brunelli** – BL scientist

M. Faure – Administrative manager

G. Wiker – Senior technician

PUBLICATIONS

Publication Rate since start-up of SNBL

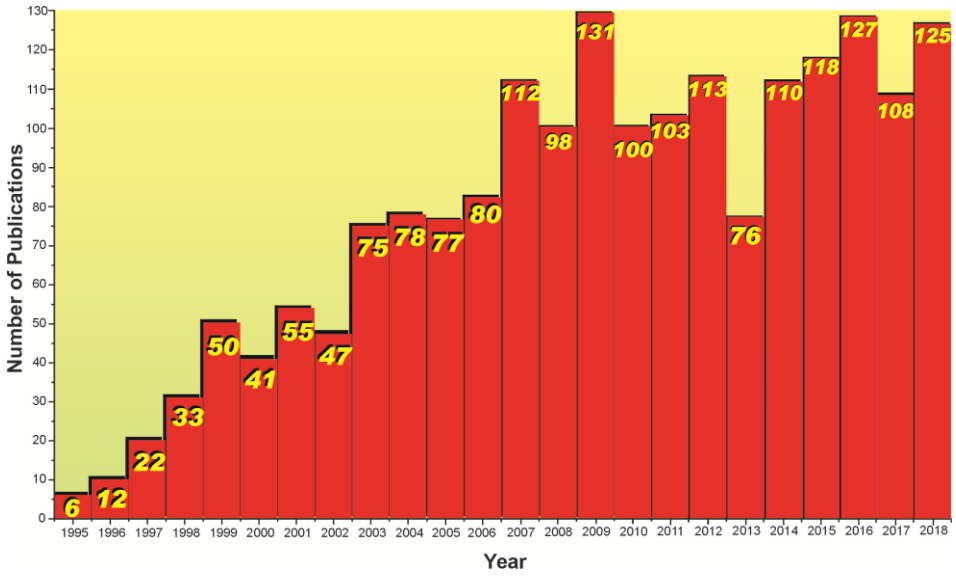

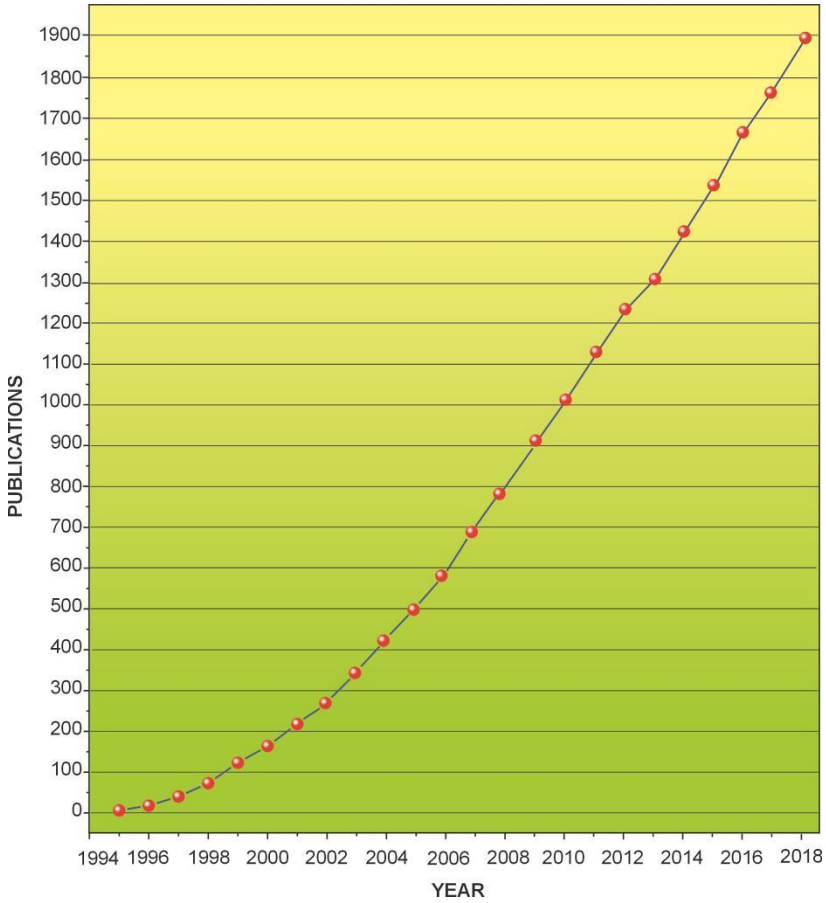

Publication rate of SNBL compared to the number of projects carried out every year

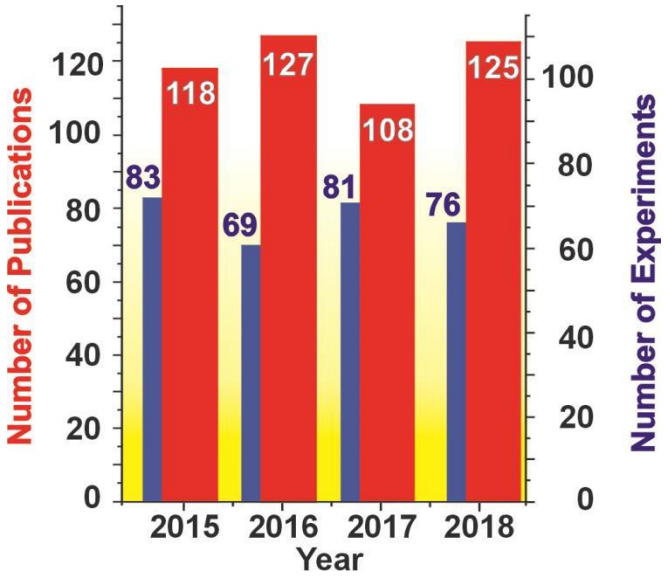

List of Publication – 2017

1. **Abeykoon, B., Grenèche, J.-M., Jeanneau, E., Chernyshov, D., Goutaudier, C., Demessence, A., Devic, Th., Fateeva, A.** *Tuning the iron redox state inside a microporous porphyrinic metal organic framework* Dalton Trans., **46**, 517-523, 2017
2. **Andersen, C.W., Borfecchia, E., Bremholm, M., Jørgensen, M.R.V., Vennestrøm, P.N.R., Lamberti, C., Lundegaard, L.F., Iversen, B.B.** *Redox-Driven Migration of Copper Ions in the Cu-CHA Zeolite as Shown by the In Situ PXRD/XANES Technique* Angewandte Chemie, **56**, 35,10367–10372, 2017
3. **Anderson, S.L., Gladysiak, A., Boyd, P.G., Ireland, C.P., Miéville, p., Tiana, D., Vlaisavljevich, B., Schouwink, P., Van Beek, W., Gagnon, K.J., Smitac, B., Stylianou, K.C.** *Formation pathways of metal–organic frameworks proceeding through partial dissolution of the metastable phase* CrystEngComm, **19**, 3407-3413, 2017
4. **Antipin, A., Alekseeva, O., Sorokina, N., Dudka, A., Voronkova, V.** *Polymorphism and structure of ion-conducting rare earth molybdates* Acta Cryst., A**73**, C902, 2017
5. **Antipin, A. M., Sorokina, N. I., Alekseeva, O. A., Dudka, A. P., Chernyshev, D. Yu., Voronkova, V. I.** *Polymorphism and structure of Nd2MO6 single crystals* Crystallography Reports, **62**, 4, 537–544, 2017
6. **Arakcheeva, A., Bykov, M., Bykova, E., Dubrovinsky, L., Pattison, Ph., Dmitriev, V., Chapuis, G.** *Incommensurate atomic density waves in the high-pressure IVb phase of barium* IUCrJ, **4**, 2, 152-157, 2017
7. **Arletti, R., Fois, E., Gigli, l., Vezzalini, G., Quartieri, S., Tabacchi, G.** *Irreversible Conversion of aWater–Ethanol Solution into an Organized Two-Dimensional Network of Alternating Supramolecular Units in aHydrophobic Zeolite under Pressure* Angewandte Chimie, **56**, 8, 2105–2109, 2017
8. **Arletti, R., Fois, E., Tabacchi, G., Quartieri, S., Vezzalini, G.** *Pressure-Induced Penetration of Water-Ethanol Mixtures in All-Silica Ferrierite* Adv. Science Letters, **23**, 6, 5966-5969, 2017

9. **Arletti, R., Giacobbe, C., Quartieri, S., Vezzalini, G.** *The Influence of the Framework and Extraframework Content on the High Pressure Behavior of the GIS Type Zeolites: The Case of Amicite* Minerals, **7**, 2, 18-31, 2017
10. **Balz, Ch., Lake, B., Reehuis, M., Nazmul Islam, A T M., Prokhnenko, O., Singh, Y., Pattison, Ph., Tóth, S**. *Crystal growth, structure and magnetic properties of* $Ca_{10}Cr_7O_{28}$ J. Physics: Condensed Matter, **29**, 22, 2017
11. **Bezrukov, A.A., Dietzel, P.D.C.** *A Permanently Porous Yttrium–Organic Framework Based on an Extended Tridentate Phosphine Containing Linker* Inorg. Chem., **56**, 21, 12830-12838, 2017
12. **Bezrukov, A. A., Törnroos, K.W., Dietzel, P.D.C.** *Modification of Network and Pore Dimensionality in Metal–Organic Frameworks Containing a Secondary Phosphine Functionality* Cryst. Growth Des., **17**, 6, 3257-3266, 2017
13. **Blagov, A. E., Vasil'ev, A. L., Dmitriev, V. P., Ivanova, A. G., Kulikov, A. G., Marchenkov, N. V., Popov, P. A., Presnyakov, M. Yu., Prosekov, P. A., Pisarevskii, Yu. V., Targonskii, A. V., Chernaya, T. S., Chernyshov, D. Yu.** *Study of the specific features of single-crystal boron microstructure* Crystallography Reports, **62**, 5, 692–702, 2017
14. **Boeije, M F J., Maschek, M., Miao, X F., Thang, N V., Van Dijk, N H., Brück, E**. *Mixed magnetism in magnetocaloric materials with first-order and second-order magnetoelastic transitions* J. Physics D: Applied Physics, **50**, 17, 174002-174023, 2017.
15. **Boeije, M.F.J., Van Eijck, L., Van Dijk, N.H., Brück, E.** *Structural and magnetic properties of hexagonal* $(Mn,Fe)_{3\text{-}delta}$ *Ga* J. Magnetism and Magnetic Materials, **433**, 297-302, 2017
16. **Bonvin, D., Arakcheeva, A., Millán, A., Piñol, R., Hofmann, H., Ebersold, M.M.** *Controlling structural and magnetic properties of IONPs by aqueous synthesis for improved hyperthermia* RSC Adv., **7**, 13159-13170, 2017
17. **Braglia, L., Borfecchia, E., Martini, A., Bugaev, A.L., Soldatov, A.V., Øien-Ødegaard, S., Bleken, B.T.L., Olsbye, U., Lillerud, K.P., Lomachenko, K.A., Agostini, G., Manzoli, M., Lamberti, C**. *The duality of UiO-67-Pt MOFs: connecting treatment conditions and encapsulated Pt species by operando XAS* Phys. Chem. Chem. Phys., **19**, 27489-27507, 2017
18. **Bräunlich, I., Mair, Ch., Bauer, M., Caseri, W.** *Structural Transitions and Thermochromism of Linear Polynuclear Cobalt(II)-4-Octadecyl-1,2,4-triazole Complexes* J. Inorganic and Organometallic Polymers and Materials, **1-7**, 2017
19. **Bruneau, A., Gustafson, K.P.J., Yuan, N., Tai, Ch.-W., Persson, I., Zou, X., Backvall, J.E.** *Synthesis of Benzofurans and Indoles from Terminal Alkynes and Iodoaromatics Catalyzed by Recyclable Palladium Nanoparticles Immobilized on Siliceous Mesocellular Foam* Chem. A Eur. J., **23**, 52, 12886–12891, 2017
20. **Bugaev, A.L., Guda, A.A., Lazzarini, A., Lomachenko, K.A., Groppo, E., Pellegrini, R., Piovano, A., Emerich, H., Soldatov, A.V., Bugaev, L.A., Dmitriev, V.P., Van Bokhoven, J.A., Lamberti, C.** *In situ formation of hydrides and carbides in palladium catalyst: When XANES is better than EXAFS and XRD* Catalysis Today, **283**, 119-126, 2017
21. **Bugaev, A.L., Guda, A.A., Lomachenko, K.A., Shapovalov, V.V., Lazzarini, A., Vitillo, J.G., Bugaev, L.A. Groppo, E., Pellegrini, R., Soldatov, A.V., Van Bokhoven, E.A., Lamberti, C**. *Core-Shell Structure of Palladium Hydride Nanoparticles Revealed by Combined X-Ray Absorption Spectroscopy and X-Ray Diffraction* J. Phys. Chem. C, **121**, 33, 18202-18213, 2017
22. **Butova, V.V., Budnyk, A.P., Guda, A.A., Lomachenko, K.A., Bugaev, A.L., Soldatov, A.V., Chavan, S.M., Øien-Ødegaard, S., Olsbye, U., Lillerud, K.P., Atzori, C., Bordiga, S., Lamberti, C.** *Modulator Effect in UiO-66-NDC (1,4-Naphthalenedicarboxylic Acid) Synthesis and Comparison with UiO-67-NDC Isoreticular Metal–Organic Frameworks* Cryst. Growth Des., **17**, 10, 5422-5431, 2017
23. **Cecot, G., Marmier, M., Geremia, S., De Zorzi, R., Vologzhanina, A.V., Pattison, Ph., Solari, E., Tirani, F.F., Scopelliti, R., Severin, K.** *The Intricate Structural Chemistry of* $M^{II}_{2n}L_n$*-Type Assemblies* J. Am. Chem. Soc., **139**, 24, 8371–8381, 2017
24. **Cerný, R., Favre-Nicolin, V., Rohlícek, J., Hušák, M.** *FOX, Current State and Possibilities* Crystals, **7**, 10, 322-333, 2017
25. **Choe, H., Heidbrink, S., Ziolkowski, M., Pietsch, J., Dyadkin, V., Gorfman, S., Chernyshov, D**. *A microcontroller for in situ single-crystal diffraction measurements with a PILATUS-2M detector under an alternating electric field* J. Appl. Cryst., **50**, 975-977, 2017
26. **Cole, J.M., Blood-Forsythe, M.A., Lin, T.Ch., Pattison, Ph., Gong, Y., Vázquez-Mayagoitia, A., Waddell, P.J., Zhang, L., Koumura, N., Mori, Ch**. *Discovery of S···C=N Intramolecular Bonding in a Thiophenylcyanoacrylate-Based Dye: Realizing Charge Transfer Pathways and Dye···TiO2 Anchoring Characteristics for Dye-Sensitized Solar Cells* ACS Appl. Mater. Interfaces, **9**, 31, 25952–25961, 2017

27. **Dalod, A.R.M., Grendal, O.G., Skjarvo, S.L., Inzani, K., Selbach, S.M., Henriksen, L., Van Beek, W., Grande, T., Einarsrud, M.-A.** *Controlling Oriented Attachment and In Situ Functionalization of TiO2 Nanoparticles During Hydrothermal Synthesis with APTES* J. Phys. Chem. C, **121**, 21, 11897-11906, 2017
28. **Dematteis, E.M., Pinatel, E.R., Corno, M., Jensen, T.R.R., Baricco, M.** *Phase diagrams in the $LiBH_4$-$NaBH_4$-KBH_4 system* Phys. Chem. Chem. Phys., **19**, 25071-25079, 2017
29. **Didelot, E., Cerný, R.** *Ionic conduction in bimetallic borohydride borate, $LiCa_3(BH_4)(BO_3)_2$* Solid State Ionics, **305**, 16-22, 2017
30. **Dovgaliuk, I., Nouar, F., Serre, Ch., Filinchuk, Y., Chernyshov, D.** *Cooperative Adsorption by Porous Frameworks: Diffraction Experiment and Phenomenological Theory* Chem. - A European J., **23**, 70, 17714-17720, 2017
31. **Dovgaliuk, I., Safin, d., Tumanov, N., Morelle, F., Moulai, A., Cerný, R., Lodziana, Z., Devillers, M., Filinchuk, Y.** *Solid Aluminum Borohydrides as Perspective Hydrogen Stores* ChemSusChem, **10,** 23, 4725-4734, 2017
32. **Duchêne, L., Kühnel, R.-S., Stilp, E., Cuervo-Reyes, E., Remhof, A., Hagemann, H., Battaglia, C.** *A stable 3 V all-solid-state sodium-ion battery based on a closo-borate electrolyte* Energy Environ. Sci., **10**, 2609-2615, 2017
33. **Efimov, V., Sikolenko, V., Troyanchuk, I. O., Karpinsky, D., Efimova, E., Tiutiunnikov, S. I., Savenko, B. N., Novoselov, D., Prabhakaran, D.** *Anomalous behavior of displacement correlation function and strain in lanthanum cobalt oxide analyzed both from X-ray powder diffraction and EXAFS data* Powder Diffraction, **32**, 51, 5151-5154, 2017
34. **El kharbachi, A., Andersen, H.F., Sørby, M.H., Vullum, P.E., Mæhlen, J.P., Hauback, B.C**. *Morphology effects in MgH_2 anode for lithium ion batteries* Int. J. Hydrogen Energy, **42**, 35, 22551-22556, 2017
35. **Engel, J., Smit, W., Foscato, M., Occhipinti, G., Törnroos, K.W., Jensen, V.R.** *Loss and Reformation of Ruthenium Alkylidene: Connecting Olefin Metathesis, Catalyst Deactivation, Regeneration, and Isomerization* J. Am. Chem. Soc., **139**, 46, 16609–16619, 2017
36. **Feng, H.L., Adler, P., Reehuis, M., Schnelle, W., Pattison, Ph., Hoser, A., Felser, C., Jansen, M**. *High-Temperature Ferrimagnetism with Large Coercivity and Exchange Bias in the Partially Ordered 3d/5d Hexagonal Perovskite $Ba_2Fe_{1.12}Os_{0.88}O_6$* Chem. Mater., **29**, 2, 886–895, 2017
37. **Fjellvåg, Ø. S., Armstrong, J., Slawinski, W.A., Sjåstad, A.O.** *Thermal and Structural Aspects of the Hydride-Conducting Oxyhydride La_2LiHO_3 Obtained via a Halide Flux Method* Inorg. Chem., **56**, 18, 11123-11128, 2017
38. **Floriano, R., Deledda, S., Hauback, B.S., Leiva, D.R., Botta, W.J.** *Iron and niobium based additives in magnesium hydride: Microstructure and hydrogen storage properties International* J.Hydrogen Energy, **42**, 10, 6810-6819, 2017
39. **Frolov, K.V., Ivanova, A.G., Chernishov, D.Y., Dovgaliuk, Y., Chareeev, D.A., Troyan, I.A**. *Crystal structure of the new superconductor FeSe1-xS* Acta Cryst., A**73**, C525, 2017
40. **Gao, S., Zaharko, O., Tsurkan, V., Su, Y., White, J.S., Tucker, G.S., Roessli, B., Bourdarot, F., Sibille, R., Chernyshov, d., Fennell, T., Loidl, A., Rüegg, Ch.** *Spiral spin-liquid and the emergence of a vortex-like state in $MnSc_2S_4$* Nature Physics, **13**, 157-161, 2017
41. **Georgopoulou, A.N., Margiolaki, I., Psycharis, V., Boudalis, A.K.** *Dynamic versus Static Character of the Magnetic Jahn–Teller Effect: Magnetostructural Studies of $[Fe_3O(O_2CPh)_6(py)_3]ClO_4 \cdot py$* Inorg. Chem., **56**, 2, 762–772, 2017
42. **GharibDoust, S.P., Brighi, M., Sadikin, Y., Ravnsbæk, D.B., Cerný, R., Skibsted, J., Jensen, T.R.** *Synthesis, Structure and Li Ion Conductivity of LiLa(BH4)3X, X = Cl, Br, I* J. Phys. Chem. C, **121,** 35, 19010-19021, 2017
43. **GharibDoust, S.P., Ravnsbæk, D.B., Cerný, R., Jensen, T.R.** *Synthesis, structure and properties of bimetallic sodium rare-earth (RE) borohydrides, NaRE(BH4)4, RE = Ce, Pr, Er or Gd* Dalton Transactions, **46**, 13421-13431, 2017
44. **Gladysiak, A., Nguyen, T.N., Navarro, J.A.R., Rosseinsky, M.J., Stylianou, K.C**. A *Recyclable Metal–Organic Framework as a Dual Detector and Adsorbent for Ammonia* Chem. Eur. J., **23,** 13602– 13606, 2017
45. **Grigor'eva, N.A., Eckerlebe, H., Eliseev, A.A., Lukashin, A.V., Napol'skii, K. S., Kraje, M., Grigor'ev, S. V.** *Structural and magnetic properties of the nanocomposite materials based on a mesoporous silicon dioxide matrix* J. Experimental and Theoretical Physics, **124**, 3, 476–492, 2017
46. **Guzik, M.N., Golasinski, K.M., Pedrosa, F. J., Jenuš, P., Bollero, A., Hauback, B.C., Deledda, S.** *Influence of ultra-short cryomilling on the microstructural and magnetic properties of cobalt ferrite* J. Alloys & Compounds, **721**, 440-448, 2017

47. **Heere, M., GharibDoust, S.H., Brighi, M., Frommen, Ch., Sørby, M.H., Cerný, R., Jensen, T.R., Hauback, B.C**. *Hydrogen Sorption in Erbium Borohydride Composite Mixtures with $LiBH_4$ and/or LiH* Inorganics **5**, 2, 31-47, 2017
48. **Heere, M., GharibDoust, S.H., Sørby, M.H., Frommen, Ch., Jensen, T.R., Hauback, B.C.** *In situ investigations of bimetallic potassium erbium borohydride* Int. J. Hydrogen Energy, **42**, 35, 22468-22474, 2017
49. **Hermann, D., Schwartz, H.A., Ruschenwitz, U.** *Crystal Structures of Z and E ortho-Tetrafluoroazobenzene* Chemistry Select, **2**, 35, 11846–11852 , 2017
50. **Hernández, W.Y., Navarro, F.A.S., Centeno, J.M.A., Vermeir, P., Van Der Voort, P.** *Structural and catalytic properties of Au/MgO-type catalysts prepared in aqueous or methanol phase: application in the CO oxidation reaction* J. Materials Science, **52**, 8, 4727-4741, 2017
51. **Hirsch, O., Kvashnina, K., Willa, Ch., Koziej, D.** *Hard X-ray Photon-in Photon-out Spectroscopy as a Probe of the Temperature-Induced Delocalization of Electrons in Nanoscale Semiconductors* Chem. Mater., **29**, 4, 1461–1466, 2017
52. **Jacot, R., Moré, R., Michalsky, R., Steinfeld, A., Patzke, G.R.** *Trends in the phase stability and thermochemical oxygen exchange of ceria doped with potentially tetravalent metals* J. Mater. Chem. A, **5**, 19901-19913, 2017
53. **Jørgensen, J.-E., Filinchuk, Y., Dmitriev, V.** *Tilting of semi-rigid GaF_6 octahedra in GaF_3 at high pressures* Powder Diffraction, **32**, 51, 569-573, 2017
54. **Kalantzopoulos, G.N., Lundvall, F., Lind, A., Arstad, B., Chernyshov, D., Fjellvåg, H., Wragg, D.S**. *SAPO-37 microporous catalysts: revealing the structural transformations during template removal* Catalysis, Structure & Reactivity, **3**, 1-2, 79-88, 2017
55. **Khalifeh, M., Saasen, A., Larsen, H.B., Hodne, H.** *Development and Characterization of Norite-Based Cementitious Binder from an Ilmenite Mine Waste Stream* Advances in Mater. Sci.& Eng., **2017**, 6849139-6849146, 2017
56. **Kim, S.M., Abdala, P.M., Margossian, T., Hosseini, D., Foppa, L., Armutlulu, A., Van Beek, W., Comas-Vives, A., Copéret, Ch., Mueller, Ch**. *Cooperativity and Dynamics Increase the Performance of NiFe Dry Reforming* Catalysts J. Am. Chem. Soc., **139**, 5, 1937-1949, 2017
57. **Kloß, S.D., Neudert, L., Döblinger, M., Nentwig, M., Oeckler, O., Schnick, W.** *Puzzling Intergrowth in Ce Nitridophosphate Unraveled by Joint Venture of Aberration-corrected STEM and Synchrotron Diffraction* J. Am. Chem. Soc., **139**, 36, 12724-12735, 2017
58. **Lange, R.Z., Hofer, G., Weber, Th., Schlüter, A.D.** *A two-dimensional polymer synthesized through topochemical [2+2]-cycloaddition on the multigram scale* J. Am. Chem. Soc., **139**, 5, 2053-2059, 2017
59. **Leontyev, I.N., Kulbakov, A.A., Allix, M., Rakhmatullin, A., Kuriganova, A.B., Maslova, O.A., Smirnova, N.V**. *Thermal expansion coefficient of carbon-supported Pt nanoparticles: In-situ X-ray diffraction study* Physica Status Solidi (b), **254**, 5, 2017
60. **Lo, C.W.T., Ortiz, B.R., Toberer, E.S., He, A., Svitlyk, V., Chernyshov, D., Kolodiazhnyi, T., Lidin, S., Mozharivskyj, Y.** *Synthesis, Structure, and Thermoelectric Properties of α-Zn_3Sb_2 and Comparison to ß-$Zn_{13}Sb_{10}$* Chem. Mater., **29**, 12, 5249–5258, 2017
61. **Lundvall, F., Wragg, D.S., Vajeeston, P., Dietzel, P.D.C., Fjellvåg, H.** *Ab initio structure solution and thermal stability evaluation of a new Ca(II) 3D coordination polymer using synchrotron powder X-ray diffraction data* CrystEngComm, **19**, 5857-5863, 2017
62. **Mašková, S., Chotard, J.-N., Denys, R.V., Miliyanchuk, K., Yartys, V., Giovannini, M., Akselrud, L., Halevy, I., Prokleška, J., Havela, L.** *$Nd_2Ni_2MgH_8$ hydride: Synthesis, structure and magnetic properties* Intermetallics, **87**, 13–20, 2017
63. **Minns, J. L. , Zajdel, P., Chernyshov, D., Van Beek, W., Green, M. A.** *Structure and interstitial iodide migration in hybrid perovskite methylammonium lead iodide* Nature Communications **8,** 15152, 2017
64. **Mikheykin, A.S., Chernyshov, D.Yu., Makarova, I.P. , Grebenev, V.V., Komornikov, V.A., Selezneva, E.V**. *Fast proton conduction in $Cs_3(HSO_4)_2(H_2PO_4)$ and $Cs_4(HSO_4)_3(H_2PO_4)$* Solid State Ionics, **305**, 30–35, 2017
65. **Møller, K.T., Fogh, A.S., Jørgensen, M., Jensen, T.R.R**. Perovskite Alkali Metal Samarium Borohydrides: Crystal Structures and Thermal Decomposition Dalton Transactions, **46**, 11905-11912, 2017
66. **Morra, E., Berlier, G., Borfecchia, E., Bordiga, S., Beato, P., Chiesa, M.** *Electronic and Geometrical Structure of Zn^+ Ions Stabilized in the Porous Structure of Zn Loaded Zeolite H-ZSM-5. A Multi-Frequency CW and Pulse EPR Study* J. Phys. Chem. C, **121**, 26, 14238-14245, 2017
67. **Nagell, M.U., Slawinski, W.A., Vajeeston, P., Fjellvåg, H., Olafsen, A.** *Temperature induced transitions in $La_4(Co_{1-x}Ni_x)_3O_{10+\delta;}$ oxygen stoichiometry and mobility* Solid State Ionics, **305**, 7–15, 2017

68. **Nentwig, M., Fahrnbauer, F., Kasprick, M., Oeckler, O.** *Single crystal structure elucidation and thermoelectric properties of a long-periodically ordered germanium arsenic telluride* J. Alloys & Compounds, **694**, 1160-1164, 2017
69. **Newton, M.A., Nicholls, R., Brazier, J.B., Nguyen, B.N., Mulligan, Ch.J., Hellgardt, K., Barreiro, E.M., Emerich, H., Hii, K.K., Snigireva, I., Thompson, P.B.J.** *Effect of retained chlorine in ENCAT™ 30 catalysts on the development of encapsulated Pd: insights from in situ Pd K, L3 and Cl K-edge XAS* Catalysis, Structure & Reactivity, **3**, 4, 149-156, 2017
70. **Novikova, K., Kuriganova, A., Leontyev, I., Gerasimova, E., Maslova, O., Rakhmatullin, A., Smirnova, N., Dobrovolsky, Y.** *Influence of Carbon Support on Catalytic Layer Performance of Proton Exchange Membrane Fuel Cells* Electrocatalysis, **9**, 1, 22-30, 2017
71. **Oertling, H., Besnard, C., Alzieu, Th., Wissenmeyer, M., Vinay, C., Mahieux, J., Fumeaux, R.** *Ionic Cocrystals of Sodium Chloride with Carbohydrates* Cryst. Growth Des., **17**, 1, 262–270, 2017
72. **Paterakis, Ch., Guo, S., Heere, M., Liu, Y., Contreras, L.F., Sørby, M.H., Hauback, B.C., Reed, D., Book, D.** *Study of the $NaBH_4$–NaBr system and the behaviour of its low temperature phase transition* Int. J. Hydrogen Energy, **42**, 35, 22538-22543, 2017
73. **Pato-Doldán, B., Rosnes, M.H., Dietzel, P.D.S.** *An in-depth structural study of the CO2 adsorption process in the porous metal-organic frameworks CPO-27-M* ChemSusChem, **10**, 8, 1710-1719, 2017
74. **Pereñíguez, R., Caballero, A., Ferri, D.** *Preferential oxidation of CO on a La-Co-Ru perovskite-type oxide catalyst* Catalysis Communications, **92**, 75-79, 2017
75. **Peng, L., Asgari, M., Miéville, P., Schouwink, P., Bulut, S., Sun, D.T., Zhou, Z., Pattison, Ph., Van Beek, W., Queen, W.L.** *Using predefined M3(μ3-O) clusters as building blocks for an isostructural series of metal-organic frameworks* ACS Appl. Mater. Interfaces, **9**, 28, 23957-23966, 2017
76. **Pisoni, A., Gaál, R., Zeugner, A., Falkowski, V., Isaeva, A., Huppertz, H., Autès, G., Yazyev, O. V., Forró, L.** *Pressure effect and superconductivity in the ß-Bi4I4 topological insulator* Phys. Rev. B **95**, 235149- 235154, 2017
77. **Polikarpov, M., Emerich, H., Klimova, N., Snigireva, I., Snigirev, A.** *Diffraction losses in monocrystalline X-ray refractive lenses* Proc. SPIE 10235, EUV and X-ray Optics: Synergy between Lab. and Space V, **102350**H, 2017
78. **Polshakov, V.I., Mantsyzov, A.B., Kozin, C.A., Adzhubei, A.A., Zhokhov, S.S., Van Beek, W., Kulikova, A.A., Indeykina, M.I., Mitkevich, V.A., Makarov, A.A.** *Novel binuclear zinc interaction fold discovered in homodimer of Alzheimer's amyloid-â fragment with Taiwanese mutation D7H* Angew. Chem. Int. Ed., **56**, 39, 11734-11739, 2017
79. **Powell, M.J., Godfrey, I.J., Quesada-Cabrera, R., Malarde, D., Teixeira, D., Emerich, H., Palgrave, R.G., Carmalt, C.J., Parkin, I.P., Sankar, G.** *Qualitative XANES and XPS Analysis of Substrate Effects in VO_2 Thin Films: A Route to Improving Chemical Vapour Deposition Synthetic Methods?* J. Phys. Chem. C, **121**, 37, 20345-20352, 2017
80. **Quaresma, S., André, V., Fernandes, A., Duarte, M.T.** *Mechanochemistry - a green synthetic methodology leading to metallodrugs, metallopharmaceuticals and bio-inspired metal-organic frameworks* Inorganica Chimica Acta, **455**, 2, 309-318, 2016
81. **Razumnaya, A.G., Mikheykin, A.S., Lukyanchuk, I.A., Shirokov, V.B., Golovko, Y.I., Mukhortov, V.M., Marssi, M.E., Yuzyuk, Y.I**. *Unexpectedly high Curie temperature in weakly strained ferroelectric film* Phys. Status Solidi, B **254**, 4, 1600413-1600420, 2017
82. **Rojo-Gama, D., Nielsen, M., Wragg, D.S., Dyballa, M., Holzinger, J., Falsig, H., Lundegaard, L.F., Beato, P., Brogaard, R.Y., Lillerud, K.P., Olsbye, U., Svelle, S.** ***A*** *Straightforward Descriptor for the Deactivation of Zeolite Catalyst H-ZSM-5* ACS Catal., **7**, 12, 8235–8246, 2017
83. **Rothensteiner, M., Bonk, A., Vogt, U.F., Emeriche, H., Van Bokhoven, J.A.** *Structural changes in equimolar ceria–hafnia materials under solar thermochemical looping conditions: cation ordering, formation and stability of the pyrochlore structure* RSC Adv., 53797–53809, 2017
84. **Rothensteiner, M., Jenni, J., Emerich, H., Bonk, A., Vogt, U.F., Van Bokhoven, J.A.** *In situ flow cell for combined X-ray absorption spectroscopy, X-ray diffraction, and mass spectrometry at high photon energies under solar thermochemical looping conditions* Review of Scientific Instruments, **88**, 083116-083166, 2017
85. **Sadikin, Y., Schouwink, P., Brighi, M., Lodziana, Z., Cerný, R.** *Modified Anion Packing of Na2B12H12 in Close to Room Temperature Superionic Conductors* Inorg. Chem., **56**, 9, 5006–5016, 2017
86. **Sadikin, Y., • Skoryunov, R.V., Babanova, O.A., Soloninin, A.V., Lodziana,• Z., Brighi, M., Skripov, A.V., Cerny. R.** *Anion Disorder in $K_3BH_4B_{12}H_{12}$ and Its Effect on Cation Mobility* J. Phys. Chem. C, **121**, 10, 5503-5514, 2017
87. **Schrade, M., Berland, K., Eliassen, S.N.H., Guzik, M.N., Echevarria-Bonet, C., Sørby, M.H., Jenus, P., Hauback, B.C., Tofan, R., Gunnæs, A.E., Persson, G., Løvvik, O.M., Finstad, T.G.** *The*

role of grain boundary scattering in reducing the thermal conductivity of polycrystalline XNiSn (X = Hf, Zr, Ti) half-Heusler alloys Scientific Reports, **7**, 13760, 2017

88. **Schwartz, H., Olthof, S., Schaniel, D., Meerholz, K., Ruschewitz, U.** *Solution-Like Behavior of Photoswitchable Spiropyrans Embedded in Metal–Organic Frameworks* Inorg. Chem., **56**, 21, 13100–13110, 2017
89. **Senn, A.-C., Kaegi, R., Hug, S.J., Hering, J.G., Mangold, S., Voegelin, A.** *Effect of aging on the structure and phosphate retention of Fe(III)-precipitates formed by Fe(II) oxidation in water* Geochimica et Cosmochimica Acta, **202**, 341-360, 2017
90. **Shemet, D.B., Pryadchenko, V.V., Srabionyan, V.V., Belenov, S. B., Mikheykin, A. S., Avakyan, L. A., Guterman, V.E., Bugaev, L. A.** *The effect of thermal treatment on the atomic structure of PtCu core-shell nanoparticles in PtCu/C electrocatalysts* J. Physics: Conference Series, **848**, 1, 2017
91. **Skorotetcky, M.S., Borshchev, O.V., Surin, N.M., Odarchenko, Y., Pisarev, S.A., Peregudova, S.M., Törnroos, K.W., Chernyshov, D., Ivanov, D.A., Ponomarenko, S.A.** *Synthesis and photostability of 1,4-bis(5-phenyloxazol-2-yl)benzene (POPOP) structural isomers and their trimethylsilyl derivatives* Dyes and Pigments, **141**, 128–136, 2017
92. **Sottmann, J., Herrmann, M., Vajeeston, P., Ruud, A., Drathen, Ch., Emerich, H., Wragg, D.S., Fjellvåg, H.** *Bismuth vanadate and molybdate: Stable alloying anodes for sodium-ion batteries* Chem. Mater., **29**, 7, 2803-2810, 2017
93. **Stefano, D. Di., Miglio, A., Robeyns, K., Filinchuk, Y., Lechartier, M., Senyshyn, A., Ishida, H., Spannenberger, S., Roling, B., Kato, Y., Hautier, G.** *Superionic diffusion through frustrated energy landscape* Cornell Univ. Library, 2017
94. **Szirmai, P., Náfrádi, B., Arakcheeva, A., Szilágyi, E., Gaál, R., Nemes, N.M., Berdat, X., Spina, M., Bernard, L., Jacimovic, J., Magrez, A., Forró, L., Horváth E.** *Cyan titania nanowires: Spectroscopic study of the origin of the self-doping enhanced photocatalytic activity* Catalysis Today, **284**, 52-58, 2017
95. **Talhi, O., Abdeldjebar, H., Belmiloud, Y., Hassaine, R., Taibi, N., Valega, M., Paz, F.A.A., Brahimi, M., Bacharia, K., Silva, A.M.S.** *Organobase catalysed one-pot exo-selective synthesis of meso-spiro[cyclohexanone-pyrandione] derivatives* New J. Chem., **41**, 10790-10798, 2017
96. **Taris, A., Grosso, M., Brundu, M., Guida, V., Viani, A.** *Application of combined multivariate techniques for the description of time-resolved powder X-ray diffraction data* J.Appl. Cryst., **50**, 2, 451-461, 2017
97. **Tedesco, C., Brunelli, M.** *X-ray Powder Diffraction* Reference Module in Chemistry, Molecular Sciences and Chemical Engineering, 45-73, 2017
98. **Trotsenko, V.G., Mikheykin, A.S., Shirokov, V.B., Razumnaya, A.G., Marssi, M. El, Gorshunov, B.P., Bush, A.A., Torgashev, V.I**. *Invar effect accompanying charge order in* $La_{0.25}Ca_{0.75}MnO_3$ Solid State Sciences, **72**, 144-149, 2017
99. **Tsakoumis, N.E., Walmsley, J.S., Rønning, M., Van Beek, W., Rytter, E., Holmen, A.** *Evaluation of Reoxidation Thresholds for* γ-Al_2O_3*-Supported Cobalt Catalysts under Fischer–Tropsch Synthesis Conditions* J. Am. Chem. Soc.,**139**, 10, 3706-3715, 2017
100. **Valkovskiy, G A ., Yashina, E G., Dyadkin, V A., Tsvyashchenko, A V., Fomicheva, L N., Bykov, M., Bykova, E., Dubrovinsky, L., Chernyshov, D Yu., Grigoriev, S.V.** *High-pressure single-crystal synchrotron diffraction study of MnGe and related compounds* J. Physics: Condensed Matter, **29**, 8, 085401-085408, 2017
101. **Van Genuchten, C.M., Peña, J.** *Mn(II) Oxidation in Fenton and Fenton Type Systems: Identification of Reaction Efficiency and Reaction Products* Environ. Sci. Technol., **51**, 5, 2982–2991, 2017
102. **Virmani, E., Beyer, O., Lüning, U., Ruschewitz, U., Wuttke, S.** *Topology-guided functional multiplicity of iron(III)-based metal–organic frameworks* Mater. Chem. Front., **1**, 1965-1974, 2017
103. **Vtyurina, D.N., Eistrikh-Geller, P.A., Kuz'micheva, G.M., Rybakov, V.B., Khramovlrina, E.V., Kaurova, A., Chernyshov, D.Y., Korchak, V.N.** *Influence of monovalent Bi+ doping on real composition, point defects, and photoluminescence in TlCdCl3 and TlCdI3 single crystals* Science China Materials, **60**, 12, 1253–1263, 2017
104. **Wehinger, B., Mirone, A., Krisch, M., Bosak, A.** *Full Elasticity Tensor from Thermal Diffuse Scattering* Phys. Rev. Lett. **118**, 035502-035510, 2017
105. **Wolczyk, A., Paik, B., Sato, T., Nervi, C., Brighi, M., GharibDoust, S.H.P., Chierotti, M., Matsuo, M., Li, G., Gobetto, R., Jensen, T.R., Cerný, R., Orimo, S., Baricco, M.** $Li_5(BH_4)_3NH$*: Lithium-Rich Mixed Anion Complex Hydride* J. Phys. Chem. C, **121**, 21, 11069-11075, 2017
106. **Xu, H.** *Constraint-induced direct phasing method* Acta Cryst., A**73**, 1, 2017
107. **Yusenko, K.V., Bykova, E., Bykov M., Gromilov, S.A., Kurnosov, A.V., Prescher, S., Prakapenka, V.B., Crichton, V.A., Hanfland, M., Margadonna, S., Dubrovinsky L.S.** *High-pressure high-*

temperature stability of hcp-IrxOs1-x (x = 0.50 and 0.55) alloys J. Alloys & Compounds, **700**, 198-207, 2017

108. **Yusenko, K.V., Bykova, E. Bykov, M., Riva, S., Crichton, W.A., Yusenko, M.V., Sukhikh, A.S., Arnaboldi, S., Hanfland, M., Dubrovinsky, L.S., Gromilov, S.A**. *Ir–Re binary alloys under extreme conditions and their electrocatalytic activity in methanol oxidation* Acta Materialia, **139**, 236–243, 2017

2018

1. **Adam, A., Poggi, M., Larquet, E., Cortès, R., Martinelli, L., Coulon, P.E., Lahera, E., Proux, O., Chernyshov, D., Boukheddaden, K., Gacoin, T., Maurin, I.** *Strain engineering of photo-induced phase transformations in Prussian blue analogue heterostructures* Nanoscale, **10,** 16030-16039, 2018
2. **Agote-Arán, M., Kroner, A., Islam, H., Slawinski, W., Wragg, D., Lezcano-Gonzalez, I., Beale, A.M.** *Determination of Molybdenum Species Evolution during Non-Oxidative Dehydroaromatization of Methane and its Implications for Catalytic Performance* ChemCatChem, **10,** 1-9, 2018
3. **Alexandropoulos, D.I., Cunha-Silva, L., Tang, J., Stamatatos, T.C.** *Heterometallic Cu/Ln cluster chemistry: ferromagnetically-coupled {Cu_4Ln_2} complexes exhibiting single-molecule magnetism and magnetocaloric properties* Dalton Transactions, **47**, 11934-11941, 2018
4. **Altynbaev, E., Siegfried, S.-A., Strauß, P., Menzel, D., Heinemann, A., Fomicheva, L., Tsvyashchenko, A., Grigoriev, S.** *Magnetic structure in $Mn_{1-x}Co_xGe$ compounds* Phys. Rev. B **97**, 144411-144420, 2018
5. **Ananias, D., Paz, F.A.A., F.A., Carlos, L.D., Rocha, J.** *Near-Infrared Ratiometric Luminescent Thermometer Based on a New Lanthanide Silicate* Chem. Eur. J., **24** ,46, 11926-11935, 2018
6. **Asanova, T., Asanov, I.P., Kim, M.G., Gorgoi, M., Sottmann, J., Korenev, S., Yusenko, K.V.** *A new approach to the study of processes of thermal decomposition and formation of nanoalloys: double complex salt $[Pd(NH_3)_4][PtCl_6]$* New J. Chem., **42,** 5071-5082, 2018
7. **Babanova, O.A., Skoryunov, R.V., Soloninin, A.V., Dovgaliuk, I., Skripov, A.V., Filinchuk, Y.** *Nuclear magnetic resonance study of hydrogen dynamics in $Al(BH_4)_4$-based hypersalts $M[Al(BH_4)_4]$ (M = Na, K, Rb, Cs)* J. Alloys & Compounds, **745**, 179-186, 2018
8. **Baekelant, W., Aghakhani, S., Coutiño-Gonzalez, E., Kennes, K., D'Acapito, F., Grandjean, D., Van der Auweraer, M., Lievens, P., Roeffaers, M.B.J., Hofkens, J., Steele, J.A.** *Shaping the Optical Properties of Silver Clusters Inside Zeolite A via Guest-Host-Guest Interactions* J. Phys. Chem. Lett., **9**, 5344-5350, 2018
9. **Bernhardt, P.V., Bilyj, J.K., Brosius, V., Chernyshov, D., Deeth, R.J., Foscato, M., Jensen, V.D., Mertes, N., Riley, M.J., Tçrnroos, K.W.** *Spin Crossover in a Hexaamineiron(II) Complex: Experimental Confirmation of a Computational Prediction* Chem. - A Eur. J., **24**, 20, 5082-5085, 2018
10. **Bezrukov, A.A., Törnroos, K.W., Le Rouxa, E., Dietzel, P.D.C.** *Incorporation of an intact dimeric Zr_{12} oxo cluster from a molecular precursor in a new zirconium metal–organic framework* Chem. Commun., **54**, 2735-2738, 2018
11. **Bissaro, B., Isaksen, I., Vaaje-Kolstad, G., Eijsink, V.G.H., Røhr, Å.K.** *How a Lytic Polysaccharide Monooxygenase Binds Crystalline Chitin* Biochemistry, **57**, 12, 1893-1906, 2018
12. **Brighi, M., Murgia, F., Lodziana, Z., Schouwink, P., Wolczyk, A., Cerny, R.** *A mixed anion hydroborate/carba-hydroborate as a room temperature Na-ion solid electrolyte* J. Power Sources, **404**, 7-12, 2018
13. **Bronwald, I., Filimonov, A., Burkovsky, R., Andronikova, D., Vakhrushev, S., Ye, Z.-G., Chernyshov, D.** *Structural Evolution in Morphotropic Lead Zirconate Titanate* IEEE Inter. Conference on Electrical Eng. and Photonics (EExPolytech), 2018
14. **Bugaev, A. L., Guda, A.A., Lomachenko, K.A., Kamyshova, E.G., Soldatov, M.A., Kaur, G., Øien-Ødegaard, S., Braglia, L., Lazzarini, A., Manzoli, M., Bordiga, S., Olsbye, U., Lillerud, K.P., Soldatov, A.V., Lamberti, C.** *Operando study of palladium nanoparticles inside UiO-67 MOF for catalytic hydrogenation of hydrocarbons* Faraday Discuss., **208**, 287-306, 2018
15. **Bugaev, A.L., Usoltsev, O.A., Guda, A.A., Lomachenko, K.A., Pankin, I.A., Rusalev, Y.V., Emerich, H., Groppo, E., Pellegrini, R., Soldatov, A.V., Van Bokhoven, J.A., Lamberti, C.** *Palladium Carbide and Hydride Formation in the Bulk and at the Surface of Palladium Nanoparticles* J. Phys. Chem. C, **122**, 22, 12029-12037, 2018
16. **Bugaev, A.L., Usoltsev, O.A., Lazzarini, A., Lomachenko, K.A., Guda, A.A., Pellegrini, R., Carosso, M., Vitillo, J.G., Groppo, E., Van Bokhoven, E., Soldatov, A.V., Lamberti, C.** *Time-resolved operando studies of carbon supported Pd nanoparticles under hydrogenation reactions by X-ray diffraction and absorption* Faraday Discuss., **208**, 187-205, 2018

17. **Bulut, S., Queen, W.L.** *Catalyst-Free Synthesis of Aryl Diamines via a Three-Step Reaction Process* J. Org. Chem., **83,** 7, 3806-3818, 2018
18. **Cambaz, M.A., Vinayan, B.P., Euchner, H., Johnsen, R.E., Guda, A.A., Mazilkin, A., Rusalev, Y.V., Trigub, A.L., Gross, A., Fichtner, M.** *Design of Nickel-Based Cation-Disordered Rock-Salt Oxides: The Effect of Transition Metal (M = V, Ti, Zr) Substitution in $LiNi_{0.5}M_{0.5}O_2$ Binary Systems* ACS Appl. Mater. Interfaces, **10**, 26, 21957–21964, 2018
19. **Cheng, H., Kvande, I., Zhu, Y., Hammer, N., Ronning, M., Walmsley, J.C., Li, P., Qi, Z., Zhou, X., De Chen** *Decoding Atomic-Level Structures of the Interface Between Pt Subnanocrystals and Nanostructured Carbon* J. Phys. Chem. C, **122**, 13, 7166-7178, 2018
20. **Chernysheva, D., Vlaic, C., Leontyev, I., Pudova, L., Ivanov, S., Avramenko, M., Allix, M., Rakhmatullin, A., Maslova, O., Bund, A., Smirnova, N.** *Synthesis of Co_3O_4/CoOOH via electrochemical dispersion using a pulse alternating current method for lithium-ion batteries and supercapacitors* Solid State Sciences, **86**, 53-59, 2018
21. **Christensen, Ch.K., Bøjesen, E.D., Sørensen, D.R., Kristensen, J.H., Mathiesen, J.K., Iversen, B.B., Ravnsbæk, D.B.** *Structural Evolution during Lithium- and Magnesium-Ion Intercalation in Vanadium Oxide Nanotube Electrodes for Battery Applications* ACS Appl. Nano Mater., **1**, 9, 5071-5082, 2018
22. **Confalonieri, G., Ryzhikov, A., Arletti, R., Nouali, H., Quartieri, S., Daou, T.J., Patarin, J.** *Intrusion-Extrusion of Electrolyte Aqueous Solutions in Pure Silica Chabazite by in Situ High Pressure Synchrotron X-ray Powder Diffraction* J. Phys. Chem. C, **122**, 49, 28001-28012, 2018
23. **De Sloovere, D., Safari, M., Elen, K., D'Haen, J., Drozhzhin, O.A., Abakumov, A.M., Šimenas, M., Banys, J., Bekaert, J., Partoens, B., Van Bael, M.K., Hardy, A.** *Reduced $Na_{2+xT}I_4O_9$/C Composite: A Durable Anode for Sodium-Ion Batteries* Chem. Mater., **30**, 23, 8521-8527, 2018
24. **Delgado, T., Enachescu, Ch., Tissot, A., Guénée, L., Hauser, A., Besnard, C.** *The influence of the sample dispersion on a solid surface in the thermal spin transition of $[Fe(pz)Pt(CN)_4]$ nanoparticles* Phys. Chem. Chem. Phys., **20**, 12493-12502, 2018
25. **Delgado, T., Enachescu, Ch., Tissot, A., Hauser, A., Guénée, L., Besnard, C.** *Evidencing size-dependent cooperative effects on spin crossover nanoparticles following their HS→LS relaxation* J. Mater. Chem. C, **6**, 12698-12706, 2018
26. **Delgado, T., Tissot, A., Guénée, L., Hauser, A., Valverde-Muñoz, F.J., Seredyuk, M., Real, J.A., Pillet, S., Bendeif, E., Besnard, C.** *Very Long-Lived Photogenerated High-Spin Phase of a Multistable Spin-Crossover Molecular Material* J. Am. Chem. Soc., **140**, 40, 12870-12876, 2018
27. **Dmitriev, V. P., Chernyshov, D. Yu., Dyadkin, V. A., Makarova, I. P., Leontyev, I. N., Andronikova, D. A., Bronwald, I., Burkovsky, R. G., Vakhrushev, S. B., Filimonov, A. V., Grigoriev, S. V.** *Crystallography Based on Synchrotron Radiation: Experiments of Russian Users of the ESRF BM01 Diffraction Beam Line* J. Synch. Investig., **12**, 3, 395–407, 2018
28. **Dos Santos, E.C., Gates, W.P., Michels, L., Juranyi, F., Mikkelsen, A., Da Silva, G.J., Fossum, J.O., Bordallo, H.N.** *The pH influence on the intercalation of the bioactive agent ciprofloxacin in fluorohectorite* Applied Clay Science, **166**, 288-298, 2018
29. **Drozhzhin, O. A., Tereshchenko, I. V., Emerich, H., Antipov, E. V., Abakumov, A. M., Chernyshov, D.** *An electrochemical cell with sapphire windows for operando synchrotron X-ray powder diffraction and spectroscopy studies of high-power and high-voltage electrodes for metal-ion batteries* J. Synchrotron radiation, **25**, 2, 2018
30. **Edalati, K., Uehiro, R., Ikeda, Y., Li, H.W., Emami, H., Filinchuk, Y., Arita, M., Sauvage, X., Tanaka, I., Akiba, E., Horita, Z.** *Design and synthesis of a magnesium alloy for room temperature hydrogen storage* Acta Materialia, **149**, 88-96, 2018
31. **El kharbachi, A., Hu, Y., Sørby, M.H., Mæhlen, Vullum, P.E., Fjellvåg, H., Hauback, B.C.** *Reversibility of metal-hydride anodes in all-solid-state lithium secondary battery operating at room temperature* Solid State Ionics, **317**, 263-267, 2018
32. **El kharbachia, A., Hu, Y., Sørby, M.H., Vullum, P.E., Mæhlen, J.P., Fjellvåg, H., Hauback, B.C.** *Understanding Capacity Fading of MgH_2 Conversion-Type Anodes via Structural Morphology Changes and Electrochemical Impedance* J. Phys. Chem. C, **122**, 16, 8759-8759, 2018
33. **El kharbachia, A., Hu, Y., Yoshida, K., Vajeeston, P., Kim, S., Sørby, M.H., Orimo, S.-i., Fjellvåg, H., Hauback, B.C.** *Lithium ionic conduction in composites of $Li(BH_4)_{0.75}I_{0.25}$and amorphous $0.75Li_2S{\cdot}0.25P_2S_5$ for battery applications* Electrochimica Acta, **278**, 232-239, 2018
34. **El Kharbachi, A., Uesato, N., Kawai, H., Wenner, S., Miyaoka, H., Sørby, M.H., Fjellvåg, H., Ichikawa, T., Hauback, B.C.** *MgH2–CoO: a conversion-type composite electrode for LiBH4-based all-solid-state lithium ion batteries †* RSC Adv., **8**, 23468-23474, 2018

35. **Frolov, K.V., Lyubutin, I.S., Alekseeva, O.A., Smirnova, E.S.. Verin, I.A., Temerov, V.L., Bezmaternykh, L.N., Gudim, I.A., Artemov, V.V., Dmitrieva, T.V.** *Dynamics of structural and magnetic phase transitions in ferroborate $YFe_3(BO_3)_4$* J. Alloys and Compounds, **748**, 989-994, 2018
36. **Gao, S., Guratinder, K., Stuhr, U., White, J. S., Mansson, M., Roessli, B., Fennell, T., Tsurkan, V., Loidl, A., Hatnean, M.C., Balakrishnan, G., Raymond, S., Chapon, L., Garlea, V. O., Savici, A. T., Cervellino, A., Bombardi, A., Chernyshov, D., Rüegg, Ch., Haraldsen, J. T., Zaharko, O.** *Manifolds of magnetic ordered states and excitations in the almost Heisenberg pyrochlore antiferromagnet $MgCr_2O_4$* Phys. Rev. B **97**, 134430-134439, 2018
37. **Gazizulina, A., Quintero-Castro, D.L., Wulferding, D., Teyssier, G., Prokes, K., Yokaichiya, F., Schilling, A.** *Tuning the orbital-lattice fluctuations in the mixed spin-dimer system $Ba_{3-x}Sr_xCr_2O_8$* Phys. Rev. B **98**, 144115 –144120, 2018
38. **Gianotti, V., Favaro, G., Bonandini, L., Palin, L., Croce, G., Boccaleri, E., Artuso, E., Van Beek, W., Barolo, C., Milanesio, M.** *Rationalization of dye uptake on titania slides for dye-sensitized solar cells by a combined chemometric and structural approach* IRISAperTO, **7**, 11, 3039-3052, 2018
39. **GharibDoust, S.P., Heere, M., Nervi, C., Sørby, M.H., Hauback, B.C., Jensen, T.R.R.** *Synthesis, Structure and Polymorphic Transitions of Praseodymium(III) and Neodymium(III) Borohydride, $Pr(BH_4)_3$ and $Nd(BH_4)_3$* Dalton Trans., **47**, 8307-8319, 2018
40. **Gigli, L., Arletti, R., Fois, E., Tabacchi, G., Quartieri, S., Dmitriev, V., Vezzalini, G.** *Unravelling the High-Pressure Behaviour of Dye-Zeolite L Hybrid Materials* Crystals, **8**, 2, 79-99, 2018
41. **Gigli, L., Arletti, R., Tabacchi, G., Fabbiani, M., Vitillo, J.G., Martra, G., Devaux, A., Miletto, i., Quartieri, S., Calzaferri, G.A., Fois, E.** *Structure and Host-Guest Interactions of Perylene- Diimide Dyes in Zeolite L Nanochannels* J. Phys. Chem. C, **122**, 6, 3401-3418, 2018
42. **Gladysiak, A., Deeg, K.S., Dovgaliuk, I., Chidambaram, A., Ordiz, K., Boyd, P.G., Moosavi, S.M., Ongari, D., Navarro, J.A.R., Smit, B., Stylianou, K.S.** *A bi-porous metal–organic framework with tuneable CO_2/CH_4 separation performance facilitated by intrinsic flexibility* ACS Appl. Mater. Interfaces, **10,** 42, 36144-36156, 2018
43. **Gladysiak, A., Nguyen, Tu N., Anderson, S.L., Boyd, P.G., Palgrave, R.G., Bacsa, J., Smit, B., Rosseinsky, M.G., Stylianou, K.S.** *Shedding Light on the Protonation States and Location of Protonated N Atoms of Adenine in Metal–Organic Frameworks* Inorg. Chem., **57**, 4, 1888–1900, 2018
44. **Gladysiak, A., Nguyen, Tu N., Spodaryk, M., Lee, J.-H., Neaton, J., Zuttel, A., Stylianou, K.S.** *Incarceration of iodine in a pyrene-based metal–organic framework* Chemistry - A Eur. J., **24**, 1-7, 2018
45. **Glätzle, M., Janka, O., Svitlyk, V., Chernyshov, D., Bartsch, M., Zacharias, H., Pöttgen, R., Huppertz, H.** *The High-Pressure Oxide Tb_3O_5 and its Non-Centrosymmetric Low-Temperature Polymorph–A Comprehensive Study* Chem. Eur. J., **24**, 15236-15243, 2018
46. **Glushkova, A., Arakcheeva, A., Pattison, P., Kollár, M., Andricevic, P., Náfrádi, B., Forró, L., Horváth, E.** *Influence of the organic cation disorder on photoconductivity in ethylenediammonium lead iodide, $NH_3CH_2CH_2NH_3PbI_4$†* CrystEngComm, **20**, 3543-3549, 2018
47. **Gomes, A.C., Antunes, M.M., Abrantes, M., Valente, A.A., Paz, F.A.A., Gonçalves, I.S., Pillinger, M.** *An Organotin Vanadate with Sodalite Topology and Catalytic Versatility in Oxidative Transformations* ChemCatChem, **10**, 16, 3481-3489, 2018
48. **Grendal, O.G., , Anders B., Blichfeld, A. B., Skjærvø, S.L., Van Beek, W., Selbach, S.M.** *Tor Grande and Mari-Ann Einarsrud Facile Low Temperature Hydrothermal Synthesis of $BaTiO_3$ Nanoparticles Studied by In Situ X-ray Diffraction* Crystals, **8**, 6, 253-270, 2018
49. **Guccione, P., Palin, L., Milanesio, M., Belviso, R.D., Caliandro, R.** *Improved multivariate analysis for fast and selecti ve monitoring of structural dynamics by in situ x-ray powder diffraction* Phys. Chem. Chem. Phys., **20**, 2175-2187, 2018
50. **Gudim, I., Lofstad, M., Van Beek, W., Hersleth, H.- P.** *High-resolution crystal structures reveal a mixture of conformers of the Gly61-Asp62 peptide bond in an oxidised flavodoxin from Bacillus cereus* Protein Science, **27**, 8, 1439-1449, 2018
51. **Gurung, N. , Leo, N., Collins, S. P., Nisbet, G., Smolentsev, G., García-Fernández, M., Yamaura, K., Heyderman, L. J., Staub, U., Joly, Y., Khalyavin, D. D., Lovesey, S. W., Scagnoli, V.** *Direct observation of electron density reconstruction at the metal insulator transition in $NaOsO_3$* Cornell University Library, 2018
52. **Guzik, M.N., Echevarria-Boneta, C., Riktor, M.D., Carvalho, P.A., Gunnæs, A.E., Sørby, M.H., Hauback, B.C.** *Half-Heusler phase formation and Ni atom distribution in M-Ni-Sn (M = Hf, Ti, Zr) systems* Acta Materialia, **148**, 216-224, 2018

53. **Heere, M., Zavorotynska, O., Deledda, S., Sørby, M.H., Book, D., Steriotis, T., Hauback, B.C.** *Effect of additives, ball milling and isotopic exchange in porous magnesium borohydride* RSC Adv., **8**, 27645-27653, 2018
54. **Heinke, F., Nietschke, F., Fraunhofer, C., Dovgaliuk, I., Schillera, J., Oeckler, O.** *Structure and thermoelectric properties of the silver lead bismuth selenides $Ag_5Pb_9Bi_{19}Se_{40}$ and $AgPb_3Bi_7Se_{14}$* Dalton Trans., **47**, 12431-12438, 2018
55. **Heinz, M., Srabionyan, V.V., Avakyan, L.A., Bugaev, A.L., Skidanenko, A.V., Pryadchenko, V.V., Ihlemann, J., Meinertz, J., Patzig, Ch., Dubiel, M.** *Formation and implantation of gold nanoparticles by ArF-excimer laser irradiation of gold-coated float glass* J. Alloys & Compounds, **736**, 152-162, 2018
56. **Hinokuma, S., Wiker, G., Suganuma, T., Bansode, A., Stoian, D., Huertas, S.C., Molina, S., Shafir, A., Rønning, M., Van Beek, W., Urakawa, A.** *Versatile IR spectroscopy combined with synchrotron XAS-XRD: Chemical, electronic and structural insights during thermal treatment of MOF materials* Eur. J. Inorg. Chem. **17**, 1847-1853, 2018
57. **Hofer, G., Grieder, F., Kröger, M., Schlüter, A. D., Weber, Th.** *Unraveling two-dimensional polymerization in the single crystal* J. Appl. Cryst., **51**, 481-497, 2018
58. **Hosseiniamoli, H., Bryant, G., Kennedy, E.M., Mathisen, K., Nicholson, D.G., Sankar, G., Setiawan, A., Stockenhuber, M.** *Understanding structure function relationships in zeolite supported Pd catalysts for oxidation of ventilation air methane* ACS Catal., **8**, 5852-5863, 2018
59. **Ibsen, C.J.S., Birkedal, H.** *Pyrophosphate-Inhibition of Apatite Formation Studied by In Situ X-Ray Diffraction* Minerals, **8,** 2, 65-72, 2018
60. **Jones, R.C., Gardiner, M.G., Skelton, B.W., Tolhurst, V-A.** *Synthesis and structural studies of dicationic Pd(II) and Pt(II) complexes of 2-(alkylchalcogenomethyl)pyridines, $[M\{NC_5H_4\text{-}2\text{-}(CH_2ER)\}_2][PF_6]_2$* Polyhedron, **156**, 291-296, 2018
61. **Jørgensen, M., Lee, Y.-S., Bjerring, M., Jepsen, L.H., Akbey, U., Cho, Y.W., Jensen, T.R.R.** *Disorder Induced Polymorphic Transitions in the High Hydrogen Density Compound $Sr(BH_4)_2(NH_3BH_3)_2$* Dalton Trans., **47**, 16737-16746, 2018
62. **Klar, P.B., Etxebarria, I., Madariaga, G.** *Exploiting superspace to clarify vacancy and Al/Si ordering in mullite* IUCRJ, **5**, 497-509, 2018
63. **Knorpp, A.J., Pinar, A.B., Newton, M., Sushkevich, V., Van Bokhoven, J.A.** *Copper-exchanged omega (MAZ) zeolite: copper-concentration dependent active sites and its unprecedented methane to methanol conversion* ChemCatChem., **10**, 24, 5593-5596, 2018
64. **Kochetygov, I., Bulut, S., Asgari, M., Queen, W.L.** *Selective CO_2 adsorption by a new metal-organic framework: synergy between open metal sites and a charged imidazolinium backbone* Dalton Trans., **47**, 10527-10535, 2018
65. **Kulbakov, A.A., Allix, M., Rakhmatullin, A., Mikheykin, A.S., Popov, Y.V., Smirnova, N., Maslova, O. Leontyev, I.N**. *In Situ Investigation of Non-Isothermal Decomposition of Pt Acetylacetonate as One-Step Size-Controlled Synthesis of Pt Nanoparticles* Phys.Status .Solidi, **215**, 23, 1800488, 2018
66. **Kulbakov, A.A., Kuriganova, A.B., Allix, M., Rakhmatullin, A., Smirnova, N.V., Maslova, O.A. Leontyev, I.N.** *Non-isothermal decomposition of platinum acetylacetonate as a cost-efficient and Size-Controlled Synthesis of Pt/C nanoparticles* Catalysis Communications, **117**, 14-18, 2018
67. **Kuriganova, A. B., Leont'ev, I.N., Maslova, O.A., Smirnova, N.V.** *Electrochemically synthesized Pt-based catalysts with different carbon supports for proton exchange membrane fuel cell applications* Mendeleev Communications, **28**, 4, 444-446, 2018
68. **Kuriganova, A. B., Leont'ev, I.N., Smirnova, N.V.** *PtIr/C Catalysts Synthesized by Electrochemical Dispersion Method for Proton Exchange Membrane Fuel Cells* Russian J. Electrochemistry, **54**, 6, 561-565, 2018
69. **Larabi, C., Merle, N., Le Quéméner, F., Rouge, P., Berrier, E., Gauvin, R.M., Le Roux, E., De Mallmann, A., Szeto, K.C., Taoufik, M.** *New synthetic approach towards well-defined silica supported tungsten bis-oxo, active catalysts for olefin metathesis* Catalysis Communications, **108**, 51-54, 2018
70. **Lastovina, T.A., Budnyk, A.P., Pimonova, Y.A., Bugaev, A.L., Fedorenko, A.G., Dmitriev, V.P.** *Step-by-step synthesis of a heteroatom-doped carbon-based electrocatalyst for the oxygen reduction reaction* Electrochem. Communications, **88**, 83-87, 2018
71. **Leontyev, I.N., Kuriganova, A.V., Rakhmatullin, M.A.A., Timoshenko, P.E., Maslova, O.A., Mikheykin, A.S. Smirnova, N.V.** *On the Evaluation of the Average Crystalline Size and Surface Area of Platinum Catalyst Nanoparticles* PSS, **255**, 10, 1800240-1800248, 2018
72. **Lo, C-W.T., Svitlyk, V., Chernyshov, D., Mozharivskyj, Y.** *The updated Zn–Sb phase diagram. How to make pure $Zn_{13}Sb_{10}$ ("Zn_4Sb_3")* Dalton Trans., **47**, 11512-11520, 2018

73. **Lomachenko, K.A., Jacobsen, J., Bugaev, A.L., Atzori, C., Bonino, F., Bordiga, S., Stock, N., Lamberti, C.** *Exact stoichiometry of Ce_xZr_{6-x} cornerstones in mixed-metal UiO-66 MOFs revealed by EXAFS spectroscopy* J. Am. Chem. Soc., **140**, 50, 17379-17383, 2018
74. **Maschek, M., You, X., Boeije, MFJ , Chernyshov, D., Van Dijk, NH., Bruck, E.** *Charge redistribution and the Magnetoelastic transition across the first-order magnetic transition in (Mn, Fe) 2 (P, Si, B)* Cornel Uni. Lib., **1808**, 10178, 2018
75. **Marafatto, F.F., Lanson, B., Peña, J.** *Crystal growth and aggregation in suspensions of δ-MnO_2 nanoparticles: implications for surface reactivity* Environ. Sci.: Nano, **5,** 497-508, 2018
76. **Mathisen, K., Kirste, K.G., Hargreaves, J.S.J., Laassiri, S., McAulay, K., McFarlane, A.R., Spencer, N.A.** *An In Situ XAS Study of the Cobalt Rhenium Catalyst for Ammonia Synthesis* Topics in Catalysis, **61**, 3-4, 225-239, 2018
77. **Mortén, M., Mentel, L., Lazzarini, A., Pankin, I.A., Lamberti, C., Bordiga, S., Crocellà, V., Svelle, S., Lillerud, K.P., Olsbye, U.** *A Systematic Study of Isomorphically Substituted H-MAlPO-5 Materials for the Methanol-to-Hydrocarbons Reaction* ChemPhysChem, **19,** 4, 484-495, 2018
78. **Møller, K.T., Jørgensen, M., Andreasen, J.G., Skibsted, J., Lodziana, Z., Filinchuk, Y., Jensen, T.R.** *Synthesis and thermal decomposition of potassium tetraamidoboranealuminate, $K[Al(NH_2BH_3)_4]$* Int. J. Hydrogen Energy, **43,** 1, 311-321, 2018
79. **Müller, R.J., Lan, J., Lienau, K., Moré, R., Triana, C.A., Iannuzzia, M., Patzke, G.R.** *Monitoring surface transformations of metal carbodiimide water oxidation catalysts by operando XAS and Raman spectroscopy* Dalton Trans., **47**, 10759-10766, 2018
80. **Naberezhnov, A. A., Alekseeva, O. A., Vanina, P. Yu., Chernyshov, D. Yu., Sysoeva, A. A., Rysiakiewicz-Pasek, E.** *Order-Parameter Temperature Dependences in Nanocomposites of Porous Glass–Sodium Nitrite* Bulletin Russian Academy of Sciences: Physics, **82**, 3, 238–241, 2018
81. **Newton, M.A., Knorpp, A.J., Pinar, A.B., Sushkevich, V.L., Palagin, D., Van Bokhoven, J.A.** *On the Mechanism Underlying the Direct Conversion of Methane to Methanol by Copper Hosted in Zeolites; Braiding Cu K-Edge XANES and Reactivity Studies* J. Am. Chem. Soc., **140**, 32, 10090–1009, 2018
82. **Nguyen, Tu N. , Capano, G., Gladysiak, A., Ebrahim, F.M., Eliseeva, S.V., Chidambaram, A., Valizadeh, B., Petoud, S., Smita, B., Stylianou, K.C.** *Lanthanide-based near-infrared emitting metal–organic frameworks with tunable excitation wavelengths and high quantum yields* Chem. Commun., **54**, 6816-6819, 2018
83. **Novikova, K., Kuriganova, A., Leontyev, I., Gerasimova, E., Maslova, O., Rakhmatullin, A., Smirnova, N., Dobrovolsky, Y.** *Influence of Carbon Support on Catalytic Layer Performance of Proton Exchange Membrane Fuel Cells* Electrocatalysis, **9**, 1, 22–30, 2018
84. **Pankin, L.A., Guda, A.A., Tumanov, N.A., Filinchuk, Y., Lomachenko, K.A., Bugaev, A.L., Guda, S.A., Shapovalov, V.V., Lamberti, C., Soldatov, A.V.** *Experimental and theoretical study of hydrogen desorption process from $Mn(BH_4)_2$* J. Alloys & Compounds, **735**, 277-284, 2018
85. **Pappas, D.K., Martini, A., Dyballa, M., Kvande, K., Teketel, S., Lomachenko, K.A., Baran, R., Glatzel, P., Arstad, B., Berlier, G., Lamberti, C., Bordiga, S., Olsbye, U., Svelle, S., Beato, P., Borfecchia, E.** *The nuclearity of the active site for methane to methanol conversion in Cu-mordenite: a quantitative assessment* J. Am. Chem. Soc., **140,** 45, 15270-15278, 2018
86. **Patanou, E., Tsakoumis, N.E., Myrstad, R., Blekkan, E.A.** *The impact of sequential H_2-CO-H_2 activation treatment on the structure and performance of cobalt based catalysts for the Fischer-Tropsch synthesis* Applied Catalysis A: General, **549**, 280-288, 2018
87. **Peña, D., Cognigni, A., Neumayer, Th., Van Beek, W., Jones, D.S., Quijada, M., Rønning, M.** *Identification of carbon species on iron-based catalysts during Fischer-Tropsch synthesis* Applied Catalysis A: General, **554**, 10-23, 2018
88. **Pena, D.Z., Jensen, L.S., Cognigni, A., Myrstad, R., Neumayer, Th., Van Beek, W., Rønning, M.** *The effect of copper loading on iron carbide formation and surface species in iron-based Fischer-Tropsch synthesis catalysts* ChemCatChem , **10**, 6, 1300-1312, 2018
89. **Pereñíguez, R., Ferri, D.** *Structural Reversibility of $LaCo_{1-x}Cu_xO_3$ Followed by In Situ X-ray Diffraction and Absorption Spectroscopy* ChemPhysChem., **19**, 15, 1876-1885, 2018
90. **Perez, M.T.D., Tissot, A., Guénée, L., Hauser, A., Valverde-Muñoz, F.J., Seredyuk, M., Real, J.A., Pillet, S., Bendeif, E., Besnard, C.** *Very long-lived photogenerated high-spin phase of a multistable spin-crossover molecular material* J. Am. Chem. Soc., **140**, 40, 12870-12876, 2018
91. **Polikarpov, M., Emerich, H., Klimova, N., Snigireva, I., Savin, V., Snigirev, A.** *Spectral X-Ray Glitches in Monocrystalline Diamond Refractive Lenses* Physica Status Solidi (b), **255**, 1, 2018
92. **Pryadchenko, V.V., Belenov, S.V., Shemet, D.V., Srabionyan, V.V., Avakyan, L.A., Volochaev, V.A., Mikheykin, A.S., Bdoyan, K.E., Zizak, I., Guterman, V.E., Bugaev, L.A.** *Effect of Thermal*

Treatment on the Atomic Structure and Electrochemical Characteristics of Bimetallic PtCu Core–Shell Nanoparticles in PtCu/C Electrocatalysts J. Phys. Chem. C, **122**, 30, 17199-17210, 2018

93. **Richter, B., Grinderslev, J.B., Møller, K.T., Paskevicius, M., Jensen, T.R.** *From Metal Hydrides to Metal Borohydrides* Inorg. Chem., **57**, 17, 10768-10780, 2018
94. **Rojo-Gama, D., Mentel, L., Kalantzopoulos, G.N., Pappas, D.K., Dovgaliuk, I., Olsbye, U., Lillerud, K.P., Beato, P., Lundegaard, L.F., Wragg, D.S., Svelle, S.** *Deactivation of Zeolite Catalyst H-ZSM-5 during Conversion of Methanol to Gasoline: Operando Time- and Space-Resolved X-ray Diffraction* J. Phys. Chem. Lett., **9**, 1324–1328, 2018
95. **Ruud, A., Sottmann, J., Vajeeston, P., Fjellvåg, H.** *Operando Investigations of Lithiation and Delithiation Processes in the $BiVO_4$ Anode Material* Phys. Chem. Chem. Phys., **20**, 29798-29803, 2018
96. **Sadikin, Y., Didelot, E., Łodziana, L., Cerný, R.** *Synthesis and crystal structure of solvent-free dodecahydro closododecaborate of nickel, $NiB_{12}H_{12}$* Dalton Trans., **47**, 5843-5849, 2018
97. **Sartori, S., Guzik, M.N., Knudsen, K.D., Sørby, M.H., Teprovich, J.A., Zidan, R., Hauback, B.C.** *Stability and Phase Formation in the $(Li/Na)_6C_{60}$–H Systems Studied by Neutron Scattering* J. Phys. Chem. C, **122**, 32, 18346-18355, 2018
98. **Santoru, A., Pistidda, C., Brighi, M., Chierotti, M.R., Heere, M., Karimi, F., Cao, H., Capurso, G., Chaudhary, A.-L., Gizer, G., Garroni, S., Sørby, M.H., Hauback, B.C., Cerný, R., Klassen, Th., Dornheim, M.** *Insights into the Rb–Mg–N–H System: an Ordered Mixed Amide/Imide Phase and a Disordered Amide/Hydride Solid Solution* Inorg. Chem., **51**, 6, 3197-3205, 2018
99. **Scarongella, M., Gadiyar, C., Strach, M., Rimoldi, L., Loiudice, A., Buonsanti, R.** *Assembly of ß-$Cu_2V_2O_7$/WO_3 heterostructured nanocomposites and the impact of their composition on structure and photoelectrochemical properties* J. Mater. Chem. C, **6**, 12062-12069, 2018
100. **Sikolenko, V.V., Molodtsov, S.L., Izquierdo, M., Troyanchuk, O., Karpinsky, D., Tiutiunnikov, S.I., Efimova, E., Prabhakaran, D., Novoselov, D., Efimov, V.** *Correlated oxygen displacements and phonon mode changes in $LaCoO_3$ single crystal* Physica B: Condensed Matter, **536**, 597-599, 2018
101. **Skjærvø, S.L., Wells, K.H., Sommer, S., Vu, T.-D., Tolchard, J.R., Van Beek, W., Grande, T., Iversen, B.B., Einarsrud, M.-A.** *Rationalization of hydrothermal synthesis of $NaNbO_3$ by rapid in situ time-resolved synchrotron X-ray diffraction* Cryst. Growth Des., **18**, 2, 770-774, 2018
102. **Skjærvø, S.L., Wells, K.H., Van Beek, W., Grande, T., Einarsrud, M.- A.** *Kinetics during hydrothermal synthesis of nanosized $K_xNa_{1-x}NbO_3$* CrystEngComm, **20**, 6795-6802, 2018
103. **Slawinski, W.A., Zacharaki, E., Fjellvåg, H., Sjåstad, A.O.** *Structural Arrangement in Close-Packed Cobalt Polytypes* Cryst. Growth Des., **18**, 4, 2316-2325, 2018
104. **Slebarski, A., Zajdel, P., Fijalkowski, M., Maska, M. M., Witas, P., Goraus, J., Fang, Y., Arnold, D. C., Maple, M. B.** *The effective increase in atomic scale disorder by doping and superconductivity in $Ca_3Rh_4Sn_{13}$* Condensed Matter, Superconductivity, 2018
105. **Smirnova, E.S., Alekseeva, O.A., Dudka, a.P., Artemov, V.V., Zubavichus, Y.V., Gudim, I.A., Bezmaterhykh, L.N., Frolova, K.V., Lyubutina, I.S.** *Crystal structure, phase transition and structural deformations in iron borate $(Y_{0.95}Bi_{0.05})Fe_3(BO_3)_4$ in the temperature range 90–500 K* Acta Cryst., B**74**, 226-238, 2018
106. **Smolders, S., Lomachenko, K.A., Bueken, B., Struyf, A., Bugaev, A.L., Atzori, C., Stock, N., Lamberti, C., Roeffaers, M.B.J., De Vos, D.E.** *Unravelling the Redox-catalytic Behavior of Ce^{4+} Metal–Organic Frameworks by X-ray Absorption Spectroscopy* ChemPhysChem, **19**, 4, 373-378, 2018
107. **Sønsteby, H.H., Bratvold, J.E., Weibye, K., Fjellvåg, H., Nilsen, O.** *Phase Control in Thin Films of Layered Cuprates* Chem. Mater., **30**, 3, 1095-1101, 2018
108. **Sprenger, P., Stehle, M., Gaur, A., Gänzler, A., Gashnikova, D., Kleist, W., Grunwaldt, J.-D.** *Reactivity of bismuth molybdates for selective oxidation of propylene probed by correlative operando spectroscopies* ACS Catal., **8**, 7, 6462-6475, 2018
109. **Steenberg Ibsen, C.J., Birkedal, H.** *Pyrophosphate-Inhibition of Apatite Formation Studied by In Situ X-Ray Diffraction* Minerals, **8**, 65-74, 2018
110. **Sushkevich, V.L., Palagin, D., Van Bokhoven, J.A.** *The Effect of the Active-Site Structure on the Activity of Copper Mordenite in the Aerobic and Anaerobic Conversion of Methane into Methanol* Angewandte Chemie, **57**, 29, 8906-8910, 2018
111. **Sushkevich, V.L., Van Bokhoven, J.A.** *Effect of Brønsted acid sites on the direct conversion of methane into methanol over copper-exchanged mordenite* Catal. Sci. Technol., **8**, 4141-4150, 2018
112. **Sun, D.T., Peng, L., Reeder, W.S., Moosavi, S.M., Tiana, D., Britt, D.K., Oveisi, E., Queen, W.L.** *Rapid, Selective Heavy Metal Removal from Water by a Metal–Organic Framework/Polydopamine Composite* ACS Cent. Sci., **4**, 3, 349-356, 2018

113. **Schwarzmüller, S., Souchay, D., Günther, D., Gocke, A., Dovgaliuk, I., Miller, S.A., Snyder, G.J., Oeckler, O.** *Argyrodite-Type $Cu_8GeSe_{6-x}Te_x$ (0 = x = 2): Temperature-Dependent Crystal Structure and Thermoelectric Properties* Z. Anorg. Allg. Chem., **64**, 24, 1915 -1922, 2018
114. **Tereshchenko, I.V., Aksyonov, D.A., Drozhzhin, O.A., Presniakov, I.A., Sobolev, A.V., Zhugayevych, A., Striukov, D., Stevenson, K.J., Antipov, E., Abakumov, A.M.** *The Role of Semilabile Oxygen Atoms for Intercalation Chemistry of the Metal-Ion Battery Polyanion Cathodes* J. Am. Chem. Soc., **140,** 11, 3994-4003, 2018
115. **Tumanova, N., Tumanov, N., Fischer, F., Morelle, F., Ban, V., Robeyns, K., Filinchuk, Y., Wouters, J., Emmerlingc, F., Leyssens, T.** *Exploring polymorphism and stoichiometric diversity in naproxen/proline cocrystals* CrystEngComm, **20**, 7308-7321, 2018
116. **Tumanova, N., Tumanov, N., Robeyns, K., Fischer, f., Fusaro, L., Morelle, F., Ban, V., Hautier, G., Filinchuk, Y., Wouters, J., Leyssens, T., Emmerling, F.** *Opening Pandora's Box: Chirality, Polymorphism, and Stoichiometric Diversity in Flurbiprofen/Proline Cocrystals* Cryst. Growth Des., **18**, 2, 954-961, 2018
117. **Udovenko, S. A., Chernyshov, D. Yu., Andronikova, D. A., Filimonov, A. V., Vakhrushev, S. B.** *The Technique of Studying X-Ray Scattering over Wide Temperature Range in an Electric Field* Physics Solid State, **60** ,5, 963-966, 2018
118. **Ulyankina, A., Leontyev, I., Avramenko, M., Denis Zhigunovc, Smirnova, N.** *Large-scale synthesis of ZnO nanostructures by pulse electrochemical method and their photocatalytic properties* Mater. Science in Semiconductor Processing, **76**, 7–13, 2018
119. **Vakhrushev S., Andronikova D.A., Chernyshov D.Y., Filimonov A.V., Udovenko S.A., Kumar N.V.R.** *X-Ray Scattering by Antiphase Ferroelectric Domain Walls in the Antiferroelectric Phase of the $PbZr_{0.985}Ti_{0.015}O_3$.* Lecture Notes in Computer Science, **11118**. Springer, Cham, 2018.
120. **Voßwinkel, D., Hoffmann, R.D., Svitlyk, V., Hermes, W., Greiwe, M., Niehaus, O., Chevalier, B., Matar, S.F., Al Alam, A.F., Nakhl, M., Ouaini, N., Pöttgen, R.** Two superstructures of $Ce_3Rh_4Ge_4$ Z. Kristallographie - Crystalline Mat., **233**, 2, 2018
121. **Yuan, N., Pascanu, V., Huang, Z., Valiente, A., Heidenreich, N., Leubner, S., Inge, A.K., Gaar, J., Stock, N., Persson, I., Martín-Matute, B., Zou, X.** *Probing the Evolution of Palladium Species in Pd@MOF Catalysts during the Heck Coupling Reaction: An Operando X-ray Absorption Spectroscopy Study* J. Am. Chem. Soc., **140**, 26, 8206-8217, 2018
122. **Yüzbasi, N.S., Abdala, P., Imtiaz, Q., Kim, S.M., Kierzkoska, A., Armutlulu, A., Van Beek, W., Müller, Ch.R.** *The effect of copper on the redox behaviour of iron oxide for chemical-looping hydrogen production probed by in situ X-ray absorption spectroscopy* Phys. Chem. Chem. Phys., **20**, 12736-12745, 2018
123. **Zakharkin, M.V., Drozhzhin, O.A., Tereshchenko, I., Chernyshov, D., Abakumov, A., Antipov, E., Stevenson, K.J.** *Enhancing Na^+ Extraction Limit Through High Voltage Activation of the NASICON-type $Na_4MnV(PO_4)_3$ Cathode* ACS Appl. Energy Mater., **1**, 11, 5842-5846, 2018
124. **Zakharov, B.A., Michalchuk, A.A.L., Morrisonc, C.A., Boldyreva, E.V.** *Anisotropic lattice softening near the structural phase transition in the thermosalient crystal 1,2,4,5-tetrabromobenzene* Phys. Chem. Chem. Phys., **20**, 8523-8532, 2018
125. **Zhang, N., Gorfman, S., Choe, H., Vergentev, T., Dyadkin, V., Yokota, H., Chernyshov, D., Wang, B., Glazer, A.M., Rena, W., Ye, Z.-G.** *Probing the intrinsic and extrinsic origins of piezoelectricity in lead zirconate titanate single crystals* J. Applied Crystallography, **57**, 5, 2018